Title

Abcc1 and Ggt5 support lymphocyte guidance through export and catabolism of S-geranylgeranyl-L-glutathione

Author

Gallman, Antonia Elizabeth

Publication Date

2021

Peer reviewed|Thesis/dissertation

Abcc1 and Ggt5 support lymphocyte guidance through export and catabolism of S-geranylgeranyl-L-glutathione

by
Antonia Gallman

DISSERTATION
Submitted in partial satisfaction of the requirements for degree of
DOCTOR OF PHILOSOPHY

in

Biomedical Sciences

in the

GRADUATE DIVISION
of the
UNIVERSITY OF CALIFORNIA, SAN FRANCISCO

Approved:

DocuSigned by:
Dean Sheppard
101CEA27F0AF442...

Dean Sheppard
Chair

DocuSigned by:
Christopher Allen
DocuSigned by:

CHRISTOPHER ALLEN

Jason Cyster
5FFFC327038A40D...

Jason Cyster

Committee Members

This dissertation is dedicated to my husband,

Joshua Lasker,

for his endless support

ACKNOWLEDGEMENTS

My time as a graduate student at UCSF has profoundly shaped my interests and passions, and I am grateful for the community that has supported my growth as a scientist.

The work described in this dissertation was done under the supervision of Dr. Jason Cyster, PhD. I first became aware of Dr. Cyster during my undergraduate studies and was impressed by the logic of his scientific work and the clarity with which he communicated it. Now as I complete my PhD, I can describe what an invaluable scientific mentor he has been for me. Dr. Cyster approaches science with a very rigorous, critical eye, and learning how to evaluate data and experimental design from him has been a key component of my graduate studies. Dr. Cyster has shaped my ability to see the big picture of a scientific endeavor, and how to make difficult decisions about what avenues to pursue in the course of a project. Perhaps the most impressive quality of Dr. Cyster however, is the time he makes for his trainees. Over the course of my PhD, he was always willing to meet with me to go over my data, even if I gave him very little heads up or if I asked to meet outside of the normal work week. Furthermore, he was respectful of my personal goals and timeline, and he made sure to support me in these goals at every turn. I will carry the lessons in rigor and mentorship that I learned from Dr. Cyster with me throughout my career.

I would also like to thank the other members of my thesis committee, Dr. Dean Sheppard and Dr. Chris Allen, for their constructive feedback and support, both in my science and in my career development. I am grateful for the time they spent critically

thinking about my project and carefully reading my writing. Additionally, I am thankful for the scientific guidance of Dr. Lewis Lanier and Dr. Matthew Spitzer as members of my qualifying exam committee, and Dr. Mark Ansel, as my mentor during my first graduate rotation here at UCSF. Finally, Dr. Heather Pua and Dr. Marlys Fassett have been encouraging and inclusive physician scientist mentors to me, and I am grateful for their time and advice.

Several scientists have strongly influenced my decision to pursue this degree before I arrived at UCSF, and I would like to thank Dr. Mark Shlomchik, Dr. Allison Campbell, Dr. Stephanie Eisenbarth and Dr. Samuele Calabro. Dr. Shlomchik accepted me into his lab as a freshman at Yale, and has always been there to support me ever since. In Dr. Shlomchik's lab, I worked with an MD-PhD student, Dr. Allison Campbell who really inspired me to become a physician scientist. She not only taught me the basics of laboratory science, from pipetting to experimental design, but also showed me how impactful working to bring science from the bench to the bedside could be. I would not have pursued this degree without her wonderful mentorship and example as a role model. Later in my time at Yale I joined the lab of Dr. Stephanie Eisenbarth, another physician scientist that has served as a key role model. Dr. Eisenbarth has an infectious passion for science, and I am extremely grateful for the mentorship she gave me, the independence she fostered in me as a scientist, and her continued support and advice. Finally, I would like to thank Dr. Samuele Calabro, a postdoctoral fellow in Dr. Eisenbarth's lab, who was a wonderful teacher, collaborator and friend with whom to do science.

During my time in the Cyster lab, I have had the privilege to work with many great colleagues that have gone out of their way to share their knowledge and expertise. I want to thank every member of the Cyster lab for their collegiality and support. I particularly want to thank Dr. Eric Dang, Dr. Lauren Rodda, and Dr. Erick Lu for their guidance and willingness to help me troubleshoot as I began new projects in the lab, and Dr. Marco de Giovanni who taught me two photon microscopy as I finished up my studies. Dr. Michelle Mintz, as a senior MD PhD student in the lab, was both a role model and friend for me, and I am extremely grateful for her encouragement and guidance, especially during the challenging portions of my degree. My baymates and fellow graduate students, Marissa Chou and Elise Wolf have been truly amazing colleagues and friends, and I will miss being able to reflect with them daily on the ups and downs of graduate school.

I have also had many engaging and fruitful scientific collaborations during my PhD, and I want to particularly thank the following people who were all outstanding teachers and collaborators: Dr. Moriah Sandy, who taught me mass spectrometry and with whom I optimized measuring GGG in tissues; Dr. David Nguyen, who taught me CRISPR editing and with whom I knocked down P2RY8 in human T cells; Dr. Oscar Aguilar, who taught me how to work with NK cells and with whom I tested many early integrin hypotheses, and Dr. Roland Wu, who taught me how to work with zebrafish and with whom I worked to examine P2RY8's role in zebrafish. I have also had a very productive international collaboration with Dr. Yuke He and Dr. Carola Vinuesa studying the contribution of P2RY8 to human disease.

Many others helped me pursue my graduate studies through their laboratory work or through the BMS and MSTP programs. Critical to the success of my experiments was the work of: Jinping An, genotyping mice and maintaining common mouse colonies; Ying Xu, aiding in molecular biology and CRISPR mouse work; and Zhongmei Li, creating several CRISPR knockout mouse lines. Bernarda Lopez, Claire Chan, Kenna Fowler and Viviana Davila helped keep the lab running smoothly and were always willing to help me track down a reagent or shipment at the last minute. Dr. Chris Allen and Dr. Qizhi Tang provided access to key mouse lines, and Dr. Joao Pereira provided advice for two photon imaging of the bone marrow. I would also like to thank the BMS and MSTP programs, including Dr. Mark Anderson, Dr. Anita Sil, Geri Ehle, Demian Sainz, Ned Molyneaux, Amanda Andonian, Andres Zepeda and my many MSTP classmates who have all helped guide me and offered me advice through the many turning points of my graduate degree.

Finally I would like to thank my family for their unwavering support. I prepared many research proposals and lab meetings from the couch of my in-laws in Reno, cheered on with snacks and good company, and I am honored to have the privilege of calling them my family. My sister as a practicing nurse has always been there to remind me about the real world of medicine, and I am grateful for her levity and her keeping me grounded during such an academic pursuit. My parents have supported my love of science always, providing me endless encouragement and unparalleled opportunities, and I am thankful for all the monumental sacrifices they have made for me over the years. Finally, my husband Joshua Lasker is truly my greatest cheerleader, and I simply could not have completed this degree without him.

CONTRIBUTIONS TO PRESENT WORK

The work described in this dissertation was done under the direct supervision of Dr. Jason Cyster, PhD. Funding for this research was acquired through the F30 NIAID as well as additional funding acquired through Dr. Cyster. Additional contributions are described below.

The presented chapters are adapted from the F30 NIAID grant “F30AI150061” and a publication under review at *Science Immunology*, “Abcc1 and Ggt5 support lymphocyte guidance through export and catabolism of S-geranylgeranyl-L-glutathione.” The thesis abstract was adapted from this work. The co-authors for this submission to *Science Immunology* were Finn Wolfreys, David Nguyen, Moriah Sandy, Ying Xu, Jinping An, Zhongmei Li, Alexander Marson, Erick Lu and Jason G. Cyster. Dr. Cyster and I conceptualized the study, designed the experiments, interpreted the results and collaboratively wrote the manuscript. I performed experiments and prepared figures for publication. Dr. Finn Wolfreys provided intellectual input, designed experiments, helped with LC-MS/MS and synthesized GGG. Dr. Erick Lu provided intellectual input and performed MK571 experiments. Dr. David Nguyen provided intellectual input and edited human T cells. Dr. Moriah Sandy provided intellectual input and performed LC-MS/MS measurements. Ying Xu, Jinping An and Zhongmei Li generated and screened knockout mice and performed PCR analysis. Dr. Alexander Marson supervised the CRISPR experiments.

Abcc1 and Ggt5 support lymphocyte guidance through export and catabolism of S-geranylgeranyl-L-glutathione

Antonia Gallman

ABSTRACT

P2RY8 promotes the confinement and growth regulation of germinal center (GC) B cells and loss of human P2RY8 is associated with B cell lymphomagenesis. Recently the metabolite S-geranylgeranyl-L-glutathione (GGG) was identified as a P2RY8 ligand. However, the mechanisms controlling GGG distribution are little understood. Here we show that gamma-glutamyltransferase-5 (Ggt5) expression in stromal cells is required for GGG catabolism and confinement of P2RY8-expressing cells to GCs. We identify ATP-binding cassette, sub-family C member-1 (Abcc1) as a GGG transporter and show that Abcc1 expression by hematopoietic cells is necessary for P2RY8-mediated GC confinement. Furthermore, we discover that P2RY8 and GGG negatively regulate trafficking of B and T cells to the bone marrow (BM). Importantly, P2RY8 loss-of-function human T cells show increased BM homing. By defining how GGG distribution is determined and identifying sites of P2RY8 activity, this work helps establish how disruptions in P2RY8 function contribute to lymphomagenesis and possibly other disease states.

TABLE OF CONTENTS

LIST OF FIGURES

LIST OF TABLES

CHAPTER 2:

CHAPTER ONE

Introduction

Germinal center (GC) B cell confinement:

As the key site for orchestrating the production of high affinity antibody, the germinal center (GC) plays an important role in mounting effective humoral immune responses. The GC is characterized by a complex, chemokine-driven organization of cells, and GC B cells are tightly confined to this anatomic space, lacking the ability to recirculate into the lymph or blood (Muppidi et al., 2014). This confinement fosters interactions of the GC B cells with supporting T follicular helper cells (Tfh) and antigen loaded follicular dendritic cells (FDCs) (Victora and Nussenzweig, 2012), and may exert population size control on the GC B cell compartment. Furthermore, confinement is hypothesized to contribute to the development of GCs as separate 'cellular islands.' By allowing separate evolution of distinct high affinity clones, these islands are thought to support the generation of an antibody response that is more diverse than would occur if the cells were freely intermixing (Cyster and Allen, 2019). The processes regulating GC B cell confinement, growth and mutation can become dysregulated, and as such, GCs are frequently the site of lymphoma origin (Leeman-Neill and Bhagat, 2018). GC derived lymphomas such as GCB-type diffuse large B cell lymphoma (DLBCL) and Burkitt lymphoma are considered systemic diseases that result in significant morbidity and mortality, with the escape of malignant GC B cells from their confined niche in the GC to distant sites such as the bone marrow being associated with poor prognosis (Sehn et al., 2011).

Through efforts to understand the factors governing the chemokine-driven organization of the GC, the Cyster lab has shown GC B cell confinement is dependent on the

migration inhibitory receptor S1PR2, as GC B cells in S1PR2 KO mice fail to cluster tightly within the GC and are instead found intermixed with follicular B cells at the interface of the GC and the follicle (Green et al., 2011). Sensing the lipid S1P, S1PR2 couples to the G protein Gα13 to signal via the RhoGEF Arhgef1 and inhibit cell migration in response to chemoattractants. Gα13- and Arhgef1-deficiency leads to a striking appearance of GC B cells in the lymph and bloodstream. Because this dissemination is not seen in S1PR2 KO mice, the Cyster lab hypothesized the existence of additional Gα13-coupled confinement receptors. Gα13, Arhgef1, and S1PR2 are all frequently mutated in human GC derived lymphomas (Muppidi et al., 2014) (Lohr et al., 2012) (Morin et al., 2013), and a search for other mutated receptors in these lymphomas identified the orphan receptor P2RY8 (Muppidi et al., 2014). P2RY8 is mutated in ~25% of GC-derived lymphomas (Muppidi et al., 2014) (Lohr et al., 2012) (Schmitz et al., 2012) (Forbes et al., 2011) and our lab demonstrated its coupling to Gα13 to promote migration inhibition. While widely conserved in vertebrates, P2RY8 lacks a sequence ortholog in rodents (Muppidi et al., 2014). However, it has been possible to study P2RY8 function by placing the human receptor in mouse cells and transferring the cells into mice. Expression of human P2RY8 on the surface of activated mouse B cells was sufficient to promote their clustering within mouse GCs, suggesting the ligand gradient to which P2RY8 responds is intact in mice (Muppidi et al., 2014). In addition to their roles in confinement, the Cyster lab has shown P2RY8 and S1PR2 act as tumor suppressors, as their activation inhibits the growth of GC B cells by repressing chemokine-induced pAkt (Muppidi et al., 2014). The importance of this molecular pathway in maintaining immune homeostasis can be underscored by the fact that

P2RY8, S1PR2, or GNA13 are mutated in approximately ~30% of GCB-DLBCL cases and ~60% of Burkitt lymphoma cases (Muppidi et al., 2014).

GGG identification and biology:

Work published in 2019 from the Cyster lab identified the endogenous ligand of P2RY8 (Lu et al., 2019). Using a bioassay to screen tissue extracts for P2RY8-dependent migration inhibition activity, bioactivity was found across many rodent and human tissues and cell lines. Biochemical fractionation coupled with LC-MS/MS revealed the ligand as the previously undescribed molecule, S-geranylgeranyl-L-glutathione (GGG). GGG consists of the isoprenoid, geranylgeranyl, conjugated to the polar tripeptide glutathione, a composition that makes it amphiphilic. Chemical synthesis and testing in migration and desensitization assays demonstrated GGG is a P2RY8 ligand of nM potency. GGG was 100-fold more active on P2RY8 than the only other defined glutathione-containing lipid mediator, leukotriene C4 (LTC4). GGG inhibited the migration of human GC B and Tfh cells and repressed chemokine induction of pAkt in GC B cells and DLBCL cells carrying intact P2RY8 genes (Lu et al., 2019). GGG was found to be abundant in liver tissue and bile. Notably, human tonsil as well as mouse spleen and lymph node (LN) extracts contained low nanomolar concentrations of GGG, indicating that it is present in lymphoid tissues at levels shown to be active on the receptor in vitro.

Glutathione conjugated lipids are often catabolized by gamma-glutamyl transferases (Ggt), peptidase-like enzymes that cleave the gamma-glutamyl bond in the glutathione

tripeptide to generate CysGly + Glu (Heisterkamp et al., 2008). Expression of the 5 Ggt family members in HEK293T cells has demonstrated Ggt5 is most active towards GGG, converting it into GG-CysGly and Glu, with Ggt1 and Ggt2 demonstrating weak activity (Lu et al., 2019). Tissue staining and in situ hybridization revealed that Ggt5 was highly expressed by human and mouse FDCs, supporting the idea that it may be a key enzyme in GGG catabolism in lymphoid tissues (Lu et al., 2019). Moreover, overexpression of Ggt5 in follicular B cells in vivo was *sufficient* to disrupt the confinement-promoting function of P2RY8: P2RY8+ cells failed to cluster with FDCs in primary follicles and in GCs (Lu et al., 2019). However, whether Ggt5 is *necessary* for establishing P2RY8-guiding GGG gradients in vivo has not been determined.

That GGG is a conjugate of glutathione and a lipid, and thus an amphiphilic molecule, implies its export from cells likely requires a specific transporter. Of the 48 ATP-binding cassette (ABC) transporters, the 12-member ABCC subfamily includes proteins specialized for efflux of glutathione-conjugated molecules (Cole, 2014). In particular, ABCC1 (MRP1) transports LTC4, oxidized glutathione (GSSG) and a range of GSH-drug conjugates (Cole, 2014). Several other family members can also transport glutathione conjugated drugs and metabolites (Slot et al., 2011). Whether any of these transporters are involved in GGG export by cells and the establishment of interstitial GGG gradients is unknown.

For the studies presented in Chapter 2, we hypothesized a model (**Figure 1.1**) in which GC confinement is achieved through the finely orchestrated distribution of GGG

throughout the follicle. Ggt5 on FDC, along with a GGG transporter and the yet undefined GGG synthesis enzyme, work to establish the GGG gradient that together with S1P promotes the confinement of GC B cells and Tfh cells to the GC.

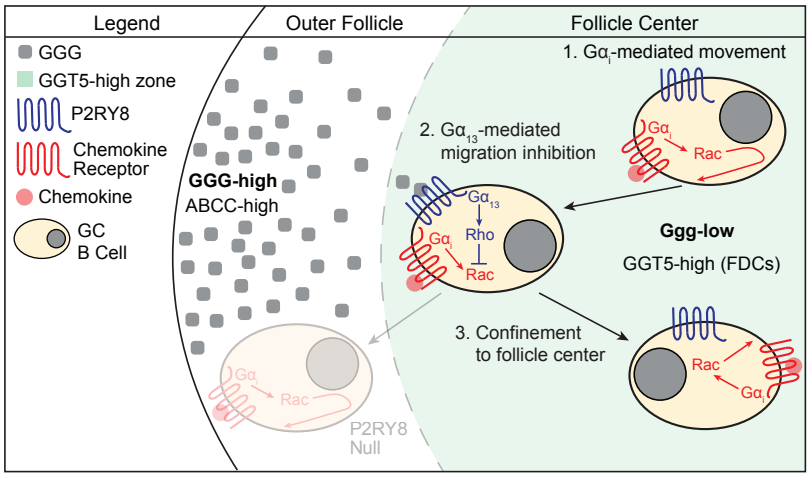

Figure 1.1: Model of P2RY8-mediated GC B-cell confinement.
ABCC+ cells and GGT5+ FDCs are suggested to work in tandem to create a follicular gradient of GGG in which GGG is more concentrated in the outer regions of the follicle, and less concentrated in the center of the follicle, or in the GC. When P2RY8-expressing GC B cells move towards the outer follicle, GGG is sensed by P2RY8. This leads to activation of Rho through Gα13, inhibiting Rac-based migration in the outward direction. As GGG does not inhibit migration towards the center of the follicle, P2RY8-expressing GC B cells are confined to this region. Adapted from (Lu and Cyster, 2019).

A potential role for GGG in mouse endogenous GC B cell confinement:

While the murine equivalent of P2RY8 has yet to be identified, evidence suggests that a second mouse Gα13-coupled receptor is working along with S1PR2 to confine GC B cells. In particular, S1PR2-mediated B cell clustering is not dependent on FDCs, yet depletion of FDCs in the mouse leads to loss of confinement of GC B cells (Wang et al., 2011). Furthermore, while S1PR2-deficiency or FDC depletion alone do not result in the dissemination of GC B cells into lymph, GC B cells do appear in the lymph when both

S1PR2 and FDC are removed (Muppidi et al., 2015). This FDC-dependent confinement acts via a Gα13-dependent mechanism, as depletion of FDCs does not lead to greater lymph dissemination in Gα13-deficient mice (Muppidi et al., 2015). Given the high expression of Ggt5 in FDCs and the dependence of transferred human P2RY8+ B cell clustering on FDCs, it can be hypothesized that Ggt5 may be responsible for supporting a confinement-generating gradient in mouse B cell follicles that acts on mouse GC B cells via a P2RY8-like receptor. GPCRs of divergent sequence sharing the same lipid ligand is not uncommon and can be found in the prostaglandin, S1P and lysosphosphatidic acid receptor families (Chun et al., 2010; Sugimoto and Narumiya, 2007). Disrupting glutathione-conjugated lipid metabolism may disrupt mouse GC B cell and Tfh cell confinement activity mediated by GGG. Thus, in addition to evaluating whether endogenous Ggt5 is responsible for regulation of GGG levels and confinement of B cells expressing human P2RY8, this dissertation will test the possible role of GGG in confinement of wild-type mouse GC B cells.

Summary:

In this work we demonstrate that Ggt5 is important for catabolism of GGG, and expression of this enzyme by stromal cells is necessary for maintaining the GGG distribution that supports P2RY8-mediated confinement of cells. We identify Abcc1 as a GGG transporter, and we show that it functions in both hematopoietic and non-hematopoietic cells to allow their production of the extracellular GGG needed for P2RY8 organizing functions. Abcc1 is also required for P2RY8 to exert a growth repressive

effect in GC B cells. Finally, we discover a new function for P2RY8 by demonstrating that it restrains lymphocyte homing to the BM.

Questions answered in this dissertation:

1. Is Ggt5 responsible for the in vivo degradation of GGG?
    - Is Ggt5 required for the P2RY8-mediated confinement of B cells to the GC?
    - What cells require Ggt5 expression to support the lymphoid GGG gradient?
2. What transporter is responsible for the export of GGG from cells in vivo?
    - Is Abcc1 required for the P2RY8-mediated confinement of B cells to the GC?
    - What cells require Abcc1 expression to support the lymphoid GGG gradient?
    - Does Abcc1 contribute to the growth repression of P2RY8-expressing cells?
    - Do alterations of the GGG gradient alter endogenous mouse B cell guidance or growth regulation?
3. Does P2RY8 affect homing of cells to other lymphoid tissues?
    - Do Ggt5 and Abcc1 affect homing of mature lymphocytes to the bone marrow?
    - Does P2RY8 alter the ability of cells to be retained in the parenchyma vs the vasculature of the bone marrow?
    - Is GGG detectable in mouse and human bone marrow?
    - Is Abcc1 required on stromal or hematopoietic cells to promote P2RY8-mediated cell exclusion from the bone marrow parenchyma?
    - Does endogenous P2RY8 on human T cells regulate bone marrow homing?

CHAPTER TWO

Results

Ggt5 is necessary for lymphoid tissue GGG catabolism:

To determine the contribution of Ggt5 to the in vivo regulation of GGG distribution we used CRISPR/Cas9 to generate mice deficient in this enzyme (**Supplementary Fig. 2.1a**). The mice were engineered to harbor an exon 1 deletion analogous to that previously shown to disrupt Ggt5 leukotrienase function in mice (Shi et al., 2001). GGG abundance was measured in bile fluid and in spleen extracts from control and Ggt5 null mice using LC-MS/MS (**Fig. 2.1a,b**). GGG is present in high amounts in bile (Lu et al., 2019) and was increased approximately two-fold upon Ggt5 deficiency (**Fig. 2.1a**). Importantly, splenic GGG increased more than eight-fold in Ggt5-deficient mice (**Fig. 2.1b**). These data establish that Ggt5 is critical in vivo for GGG catabolism, especially within lymphoid tissue.

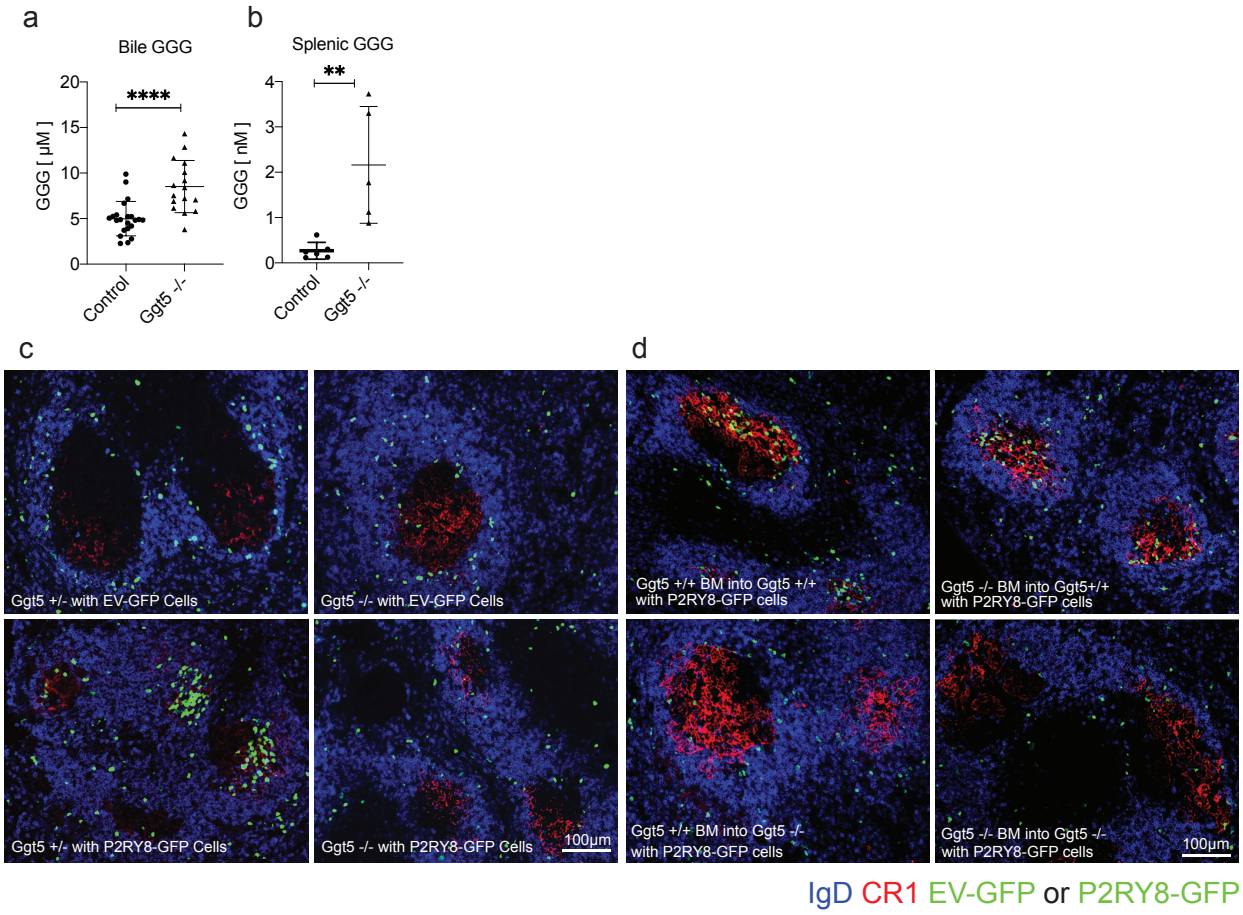

Figure 2.1: Ggt5 is required for catabolizing tissue GGG and for P2RY8-mediated follicle center confinement of B cells.
(a-b) GGG was measured in the bile (a) and spleen (b) of Ggt5-/- and control (Ggt5+/+ and +/- littermates) by LC-MS/MS. For bile n=22 control and n=16 Ggt5-/-. Spleens were pooled in groups of five (n=6 control, n=5 Ggt5-/-). (c-d) Empty vector (EV) and P2RY8-transduced activated splenic B cells were transferred into preimmunized Ggt5 +/- or -/- mice (c), or Ggt5 BM chimeric mice 8 weeks following reconstitution (d). Immunofluorescence for P2RY8- or EV-transduced B cells (GFP, green) in the splenic GC (CR1, red) of sheep red blood cell (SRBC) immunized mice relative to endogenous follicular B cells (IgD, blue). Scale bars 100µm. Data are pooled from one (a) or three (b) experiments; or representative of six (c) or two (d) biological repeats, with approximately 40 GCs visualized per biological repeat. P-values determined by unpaired two-tailed Student's t-test (a,b) *P<0.05, **P<0.01, ***P<0.001, ****P<0.0001. Graphs depict mean with s.d. and points represent biological replicates.

We next tested whether Ggt5 was required for P2RY8-mediated confinement of B cells to the GC. We hypothesized that loss of Ggt5 would disrupt the established GGG gradient throughout the follicle, eliminating regions of low GGG maintained by active degradation. This alteration would be expected to compromise the ability of P2RY8 to confine cells to the GC. B cells retrovirally transduced to express P2RY8 were transferred into either pre-immunized Ggt5-deficient or wildtype control mice and were examined for their localization in the spleen one day later. While empty vector (EV)-transduced control cells were found throughout the IgD+ region of the follicle, P2RY8 expressing cells clustered tightly over the FDC-rich region of the GC of wildtype mice as expected (**Fig. 2.1c** and **Supplementary Fig. 2.1b**). In contrast, when P2RY8+ cells were transferred into Ggt5-deficient mice, the cells failed to cluster in the GC (**Fig. 2.1c** and **Supplementary Fig. 2.1b**). A loss of P2RY8+ cell confinement in GCs was also seen in the mesenteric LNs (mLNs) (**Supplementary Fig. 2.1c**). Additionally, the confinement of P2RY8+ cells to the FDC network in the center of primary follicles of unimmunized mice was also Ggt5-dependent (**Supplementary Fig. 2.1d**). These data provide strong evidence that Ggt5-mediated catabolism of GGG is required for P2RY8 function in guiding B cell distribution within follicles across multiple lymphoid tissues and immunization states.

Ggt5 has also been shown to degrade leukotriene C4 (LTC4), a further glutathione-conjugated lipid that acts as an intercellular signaling molecule (Carter et al., 1997) (Hayes et al., 2004). LTC4 has two well established high affinity receptors (CysLTR1 and CysLTR2) (Shimizu, 2009). Using a bioassay with nanomolar sensitivity we

previously observed in vitro that LTC4 also has activity on P2RY8, though with a 100-fold less potency than GGG (Lu et al., 2019). To exclude the possibility that the lack of P2RY8+ cell clustering identified in Ggt5-deficient mice was due to an effect on LTC4 rather than GGG, we performed transfers of P2RY8+ cells into mice deficient in arachidonate 5-lipoxygenase, or 5-LO, which lack the ability to generate LTC4 (Chen et al., 1994). P2RY8+ cells transferred into pre-immunized 5-LO-deficient mice continued to cluster over the FDC network in the GC (**Supplementary Fig. 2.1e**) excluding a role for LTC4 in this process.

Ggt5 is expressed highly by FDCs in both human tonsil and mouse lymphoid tissues (Lu et al., 2019). To determine if expression of Ggt5 was required in the stromal compartment for the clustering of P2RY8+ cells, we generated chimeric mice in which Ggt5 sufficient or deficient BM was transferred into Ggt5 sufficient or deficient irradiated hosts and the mice were allowed to reconstitute. Transferred P2RY8+ B cells failed to cluster in the splenic and lymph node GC of mice lacking Ggt5 in the radioresistant, stromal compartment, but not in mice lacking Ggt5 in the hematopoietic compartment (**Fig 2.1d** and **Supplementary Fig 2.1f**). These data support a model in which Ggt5 expression by radioresistant FDCs in vivo acts to degrade local GGG, allowing for the confinement of P2RY8 expressing cells to the GC.

Abcc1 is a GGG transporter:

Owing to glutathione's polarity, glutathione conjugates generally rely on active transport, rather than passive diffusion, to leave cells. Other glutathione conjugated molecules are

transported by members of the Abcc family (Cole, 2014). Of the family's 11 members, Abcc1, Abcc4, Abcc5, and Abcc9 are highly expressed in mouse lymphoid tissue (**Supplementary Fig 2.2a**). Previous work established the production of GGG by several human cell lines, including HEK293T cells (Lu et al., 2019), which express high levels of Abcc1, Abcc4, Abcc5, and Abcc10 (**Supplementary Fig 2.2b**). MK-571 is an inhibitor of Abcc1, though with low specificity (Koley and Bard, 2012). When HEK293T cells were cultured in the presence of MK-571, the ability of the culture supernatants to inhibit P2RY8+ cell migration to CXCL12 was reduced (**Fig 2.2a** and **Supplementary Fig 2.2g**), suggesting a potential role for Abcc1 in GGG export. We then made Abcc1-deficient mice by using CRISPR/Cas9 to delete a segment of the gene previously shown to be essential for Abcc1 protein expression in mice (Lorico et al., 1997) (**Supplementary Fig 2.2c**). These mice allowed us to assay production of GGG by Abcc1-deficient cells. GGG was detected at significantly reduced concentrations in the supernatants of stimulated Abcc1-deficient B cells compared to wildtype B cells (**Fig 2.2b).** These data strongly support the conclusion that Abcc1 functions as a GGG transporter. Attempts to detect alterations in GGG abundance in lymphoid tissues of Abcc1-deficient mice were confounded by the very low amounts present in these tissues in wild-type mice and by an inability to sample selectively the interstitial space. Analysis of bile collected from Abcc1-deficient mice showed a trend towards decreased GGG that did not reach significance (**Supplementary Fig 2.2d**) suggesting that additional transporters may contribute to GGG export in the liver.

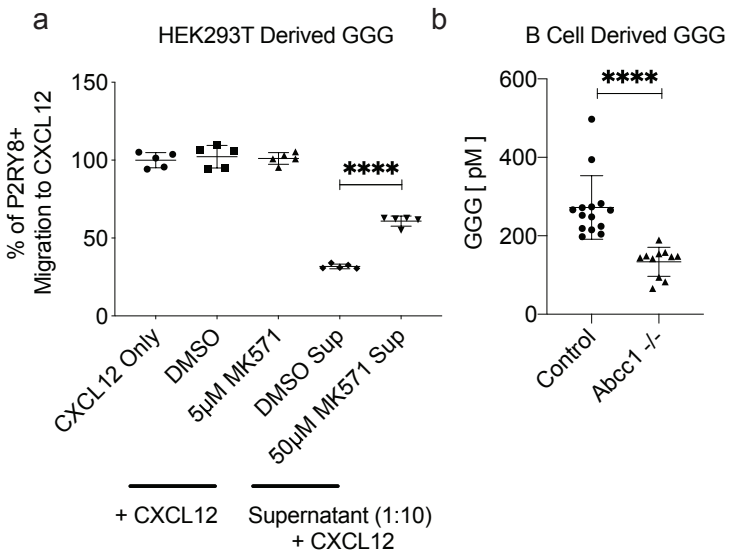

Figure 2.2: Abcc1 is required for GGG export.
(a) HEK293T cell cultures were treated with 50μM of Abcc1 inhibitor MK571 or the diluted carrier (DMSO) for 16hr. Collected supernatant was used at a 1:10 dilution in a bioassay based on the transwell migration of P2RY8+ WEHI cells towards CXCL12. Control wells contained CXCL12, CXCL12 + DMSO, or CXCL12 + 5μM MK571. (b) Activated, purified splenic B cells from Abcc1-/- and control (Abcc1+/+ and +/- littermate) mice were incubated for 72hrs, after which the supernatant was collected and measured for GGG by LC-MS/MS (n= 14 control, n=11 Abcc1-/-). Data are pooled from (b) or representative of (a) three (b) experiments. P-values determined by unpaired two-tailed Student's t-test (a,b). *P<0.05, **P<0.01, ***P<0.001, ****P<0.0001. Graphs depict mean with s.d. and points represent (a) technical or (b) biological replicates.

To evaluate the role of Abcc1 in shaping the lymphoid tissue GGG gradient, P2RY8-expressing B cells were transferred into Abcc1-deficient mice and their littermate controls. P2RY8+ B cells failed to localize to the GCs of pre-immunized Abcc1-deficient mouse spleens and LNs and instead were found throughout the IgD+ region of the B cell follicle, a region P2RY8+ cells are normally excluded from (**Fig 2.3a**, **Supplementary Fig 2.2e,f**). The distribution of P2RY8+ cells in Abcc1-deficient mice mimicked the distribution of empty vector expressing control cells. These data indicate that Abcc1 has a non-redundant role in establishing the extracellular GGG distribution needed for P2RY8 function in B cell follicles.

B cells are an important source of GGG:

We took advantage of the critical role of Abcc1 in GGG export to determine the GGG-producing cell types necessary for follicle-center confinement of P2RY8-expressing cells. We generated chimeric mice in which Abcc1 sufficient or deficient BM was transferred into Abcc1 sufficient or deficient irradiated hosts. P2RY8+ cells failed to cluster in the GCs of chimeric mice lacking Abcc1 in their hematopoietic compartment, but were able to localize in these regions in mice lacking Abcc1 only in their stromal compartment (**Fig 2.3b**, **Supplementary Fig 2.3a,b**), indicating hematopoietic Abcc1 is both necessary and sufficient for this GC localizing behavior. Interestingly, in mice lacking Abcc1 in the hematopoietic compartment, but with functional Abcc1 in the stromal compartment, P2RY8+ cells failed to localize in the GC, but were not distributed evenly throughout the IgD+ follicle like empty vector cells or P2RY8+ cells transferred into completely Abcc1-deficient mice. Instead, these P2RY8+ cells were often found at the interface of the follicle and GC, ringing this region. This discrepancy between the P2RY8+ cell localizing patterns in full Abcc1-deficient mice and mice with functional Abcc1 in their stromal compartment was especially clear when higher numbers of P2RY8+ cells were transferred (**Supplementary Fig 2.3a**). This finding provides evidence that stromal cells are capable of exporting GGG and contributing to its overall distribution in tissue.

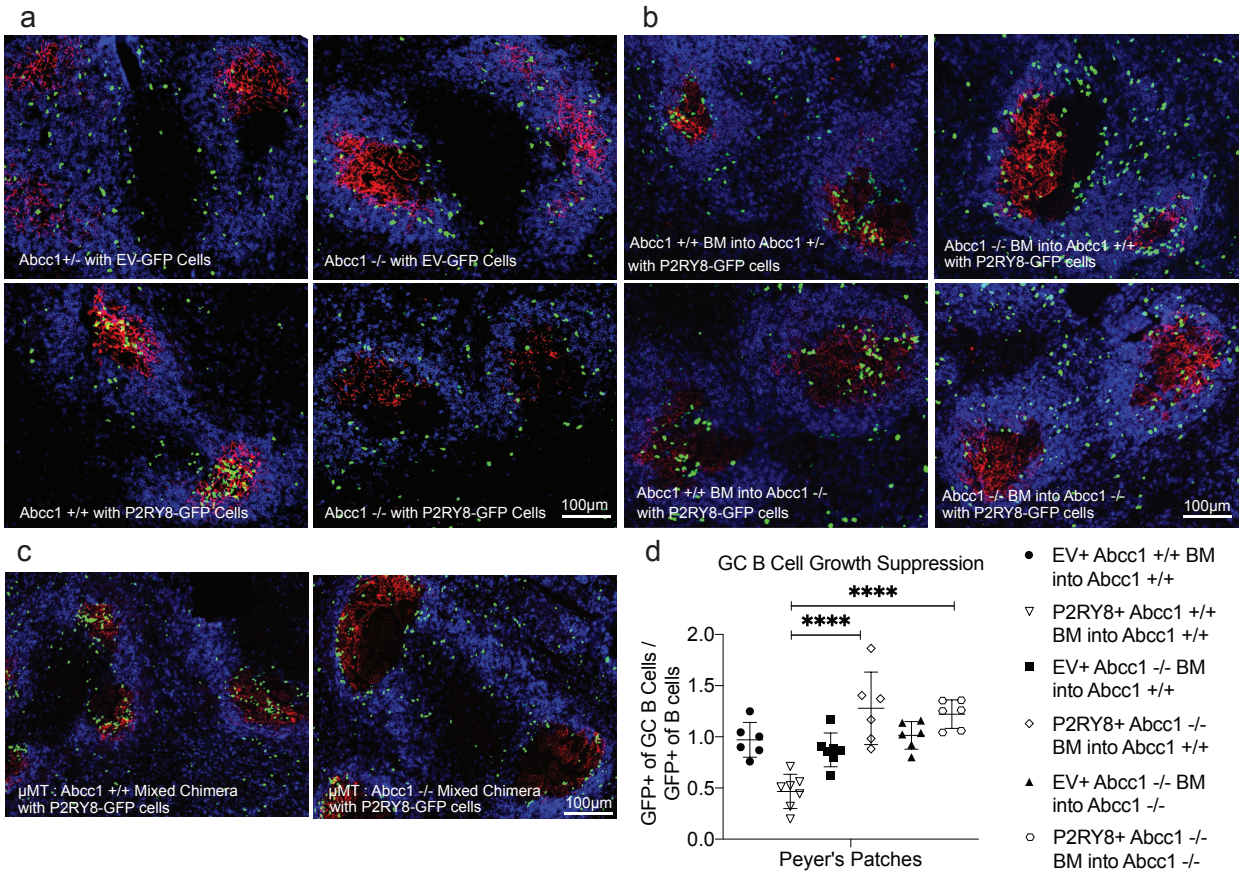

Figure 2.3: Abcc1 expression by B cells is required for P2RY8-mediated follicle center confinement and for the growth regulation of P2RY8-expressing GC B cells.

(a-c) Activated EV- or P2RY8-transduced polyclonal B cells were transferred into preimmunized Abcc1 +/+, +/- or -/- mice (a), into preimmunized BM chimeric mice of the type indicated (b), or into preimmunized Abcc1+/+ mice reconstituted with μMT BM mixed at a 3:1 ratio with Abcc1+/+ or -/- BM. (c). Immunofluorescence for P2RY8- or EV-transduced B cells (GFP, green) in the GCs (CR1, red) of SRBC immunized mice relative to endogenous follicular B cells (IgD, blue). Scale bars 100μm. (d) Irradiated Abcc1+/+ or -/- mice were reconstituted with P2RY8-GFP or EV-GFP transduced Abcc1+/+ or -/- BM. Following reconstitution, PPs were analyzed for the frequency of GFP+ cells in the follicular and GC B cells compartment. The ratio of GFP+ cells in the GC B cells vs in the follicular B cells was plotted (n=6-7, exact number shown by number of symbols in the plot). Data are pooled from two experiments and representative of four experiments (d); or representative of four (a,b,c) biological repeats, with approximately 40 GCs visualized per biological repeat. P values determined by one-way ANOVA with Tukey's multiple comparisons test (d). *P<0.05, **P<0.01, ***P<0.001, ****P<0.0001. Graphs depict mean with s.d. and points represent biological replicates.

To determine if B cell expression of Abcc1 was necessary for GGG gradient generation, we made mixed chimeras using BM from μMT mice, which lack the ability to generate mature B cells. The μMT BM was mixed in a 3 to 1 ratio with Abcc1 sufficient or deficient BM to produce mice in which Abcc1 was completely absent from B cells, but present on other hematopoietic cell types and stromal cells. P2RY8+ cells failed to cluster in the GC of these mice, instead ringing the GC region, as was seen in mice lacking Abcc1 in all but their stromal compartment (**Fig 2.3c** and **Supplementary Fig 2.3c,d**). These data indicate that B cells are the major hematopoietic source of GGG within lymphoid follicles.

Previous work showed that P2RY8 expression in GC B cells leads to a suppressive effect on GC B cell growth, particularly in mouse Peyer's patches (PPs) and mLNs (Muppidi et al., 2014). It is the loss of this growth repressive effect that likely underlies the connection between P2RY8 mutations and development of BL and GCB-DLBCL in humans. Using chimeric mice generated with P2RY8-transduced BM, we found this effect to be dependent on Abcc1, with the loss of Abcc1 in the hematopoietic compartment being sufficient for abrogation of the GC B cell growth-repression phenotype in PPs (**Fig 2.3d**). We detected only a slight P2RY8-mediated suppressive effect on GC B cells in the spleen, but this also appeared Abcc1-dependent (**Supplementary Fig 2.4a**). The effect of P2RY8 on GC B cells in mLNs was more variable but again there was evidence of an Abcc1-dependent repressive effect (**Supplementary Fig 2.4b,c**). Interestingly, the PP and mLN data show evidence of P2RY8 expression conferring a GC growth advantage when Abcc1 is selectively lacking

in hematopoietic cells. Taking this finding together with the observation that P2RY8+ B cells tend to position at the perimeter of GCs in BM chimeras of this type (**Fig 2.3b,c** and **Supplementary Fig 2.3c,d**), we speculate that this location may be advantageous for GC cell growth. Overall, these data provide in vivo evidence that the growth regulatory actions of P2RY8, like the confinement actions, depend on engagement with GGG.

Disruption of the GGG gradient does not alter confinement of endogenous mouse B cells:

P2RY8 is located on a portion of the pseudoautosomal region of the X chromosome that has been lost in rodents (Muppidi et al., 2014). With mice lacking a sequence orthologue of P2RY8, alterations of the GGG gradient may not be predicted to alter endogenous mouse B cell guidance or growth regulation. However, it remains possible that they respond to GGG through a distinct receptor. We therefore examined whether confinement of endogenous GC B cells was altered in Ggt5 or Abcc1 deficient mice. Previous work in mice lacking the GC confinement receptor S1PR2 or the downstream Gα13 protein has shown that one measure of reduced confinement is the increased presence of IgD+ follicular B cells within the GC (Green et al., 2011; Muppidi et al., 2014). Staining of mLNs of Ggt5 and Abcc1 deficient mice showed that there was no increase in IgD+ cells in the GC compared to wild-type controls (**Supplementary Fig 2.5a**). Sections from S1PR2 deficient control mice demonstrated the expected intermixing of follicular and GC B cells (**Supplementary Fig 2.5a**). Mice lacking Gα13 (but not S1PR2) suffer an extent of GC deconfinement that is sufficient to cause

dissemination of GC B cells into the lymph (Muppidi et al., 2014). Ggt5 and Abcc1 deficient mice, as well as Abcc1 chimeric mice, showed normal GC B cell frequencies upon sheep red blood cell (SRBC) immunization (**Supplementary Fig 2.5b,c**), and no dissemination of GC B cells into the lymph (**Supplementary Fig 2.5d**). We also tested the effect of combined loss of S1PR2 and disruption of the GGG gradient. Chimeric mice lacking S1PR2 in their hematopoietic compartment and Ggt5 in their radioresistant compartment showed no increased dissemination of GC B cells into the lymph compared to S1PR2-deficient control animals (**Supplementary Fig 2.5d**). These findings suggest that there is not a direct role for Ggt5 or Abcc1 in GC confinement of mouse B cells.

P2RY8 and GGG restrain lymphocyte homing to bone marrow:

In the course of evaluating the role of the GGG gradient in lymphoid organs via the transfer of P2RY8 expressing cells, we noted that activated P2RY8+ polyclonal B cells were less represented in the BM after 24hrs compared to their initial cell representation upon transfer into the mouse (**Fig 2.4a**). This effect was not seen in the blood after 24hrs (**Fig 2.4b**), and when the representation of P2RY8 cells was compared between the blood and BM of individual animals, there was a clear defect in the homing of P2RY8+ cells to the BM (**Fig 2.4c**). Polyclonal P2RY8+ B cells were also less likely to be present in the spleen after 24hrs, though this difference was of a smaller magnitude than that seen in the BM (**Supplementary Fig 2.6a**). P2RY8+ cell homing to inguinal or mLNs was comparable to the vector control cells (**Supplementary Fig 2.6b,c**). This notably decreased homing to the BM was not unique to B cells, as activated P2RY8-

transduced polyclonal CD4+ and CD8+ T cells were also less likely to be found in the BM in comparison to control cells, at both 24hrs and 5 days following transfer (**Fig 2.4a,b,c** and **Supplementary Fig 2.6d,e,f**). While there was a decrease in P2RY8+ CD8+ T cell representation in the blood at 24hrs, this difference reversed after 5 days, and the representation of P2RY8+ cells in the BM compared to the blood for CD8+ T cells was consistent with the other lymphocytes examined. Furthermore, the inhibition of BM homing was dependent on the downstream effector of P2RY8, Gα13, as P2RY8-transduced B cells from mice deficient in this G protein demonstrated equal ability to home to the BM compared to empty vector control cells (**Supplementary Fig 2.6g**). The homing defect of P2RY8+ cells was furthermore not unique to in vitro activated B or T cells, as in chimeric mice reconstituted with P2RY8 transduced BM, P2RY8+ mature B cells, T cells, and NK cells were all less represented in the BM compared to the blood (**Fig 2.4d**).

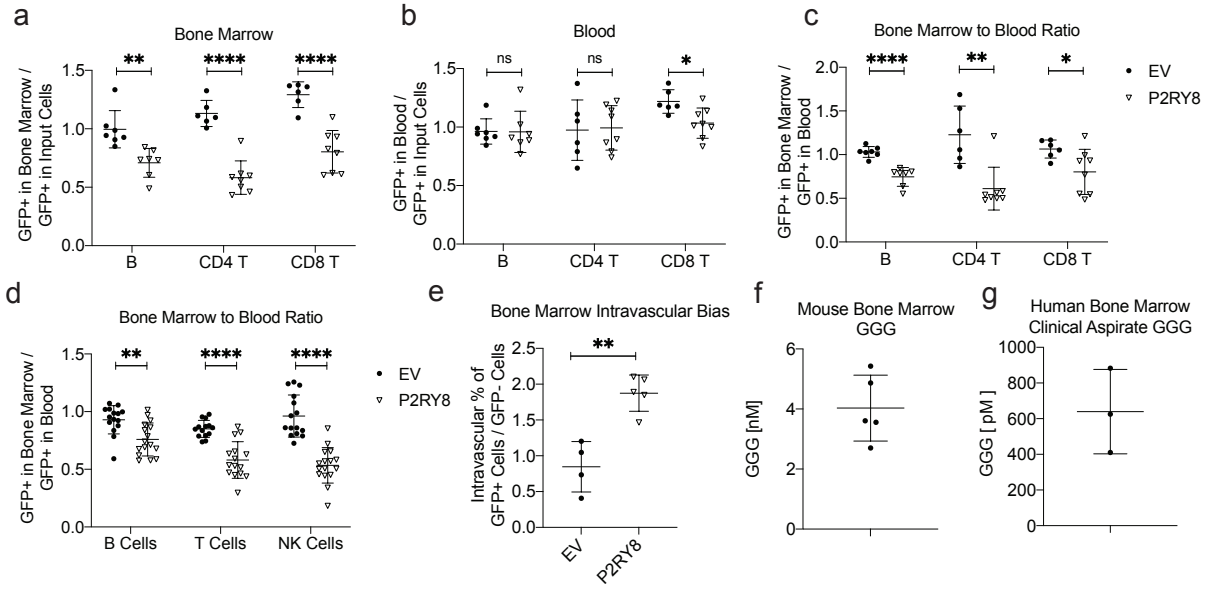

Figure 2.4: P2RY8 expression reduces lymphocyte homing to the BM.

(a-c,e) Activated EV- or P2RY8-transduced B cells or T cells were transferred into preimmunized mice. GFP frequency in the BM (a) or blood (b) after 24hrs is plotted as a ratio of the GFP frequency at the time of transfer into mice (input cells). (c) GFP frequency in the BM divided by GFP frequency in the blood (n=6-8). (d) GFP+ frequency of mature B, T and NK cells in the BM divided by GFP+ frequency in the blood in congenically marked mice reconstituted with EV or P2RY8 transduced BM (n=14-16 per group). (e) Percentage of GFP+ transferred B cells in each mouse staining with CD45.2-PE injected intravascularly, divided by GFP- transferred B cells staining for the same (n=4-5). (f,g) GGG measurement via LC-MS/MS of mouse BM (n=5) (f) or human BM aspirate (n=3) (g). Data are pooled from five (B cells in a-c, e), two (T cells in a-c), three (B and NK cells in d, and g), four (T cells in d) experiments; or representative of three (f) experiments. P values determined by unpaired two-tailed Student's t-test. *P<0.05, **P<0.01, ***P<0.001, ****P<0.0001. Graphs depict mean with s.d. and points represent biological replicates.

While fewer P2RY8+ cells homed to the BM overall, the P2RY8+ polyclonal B and T cells that did migrate to the BM were roughly two-fold more likely to be found associated with the BM vasculature rather than in the BM parenchyma, based on their rapid in vivo

staining with intravenously injected anti-CD45-PE (**Fig. 2.4e** and **Supplementary Fig 2.6h,i**). This quantification was also supported by two photon imaging of calvarial BM, where P2RY8+ cells were more abundant in locations overlapping with the vasculature (**Supplementary Fig 2.7a,b**). This finding suggests an inhibitory effect of P2RY8 as cells transit from the vasculature and make their way into the BM parenchyma. Mass spectrometry analysis of total mouse BM (cells and any interstitial fluid) established that GGG was detectable (**Fig. 2.4f**, **Supplementary Fig 2.7d**). An analysis of cell-free human BM aspirates drawn from three healthy donors established that GGG was also present in the interstitial space of human BM (**Fig 2.4g** and **Supplementary Fig 2.7e**). The difference in the amount of GGG detected in mouse and human BM most likely reflects the presence of considerable transudated plasma in the human aspirates. We were unable to detect GGG in human plasma by mass spectrometry. In accord with local production of GGG, many hematopoietic cells (as well as recirculating lymphocytes) in mouse BM (Immgen.org) and human BM (Human Cell Atlas scRNAseq (Hay et al., 2018)) express Abcc1 (**Supplementary Fig 2.7c**). Notably, P2RY8 was also expressed by many hematopoietic cells within human BM, while Ggt5 was strongly expressed by BM stromal cells.

To determine whether the decreased BM homing of P2RY8+ cells was dependent on GGG, polyclonal B cells expressing P2RY8 or empty vector were transferred into mice deficient in Ggt5 or Abcc1. Interestingly, P2RY8+ cells in mice deficient in Ggt5 showed a further reduced ability to home to the BM (**Fig. 2.5a**), perhaps reflecting stronger inhibition of P2RY8+ cell entry due to elevated tissue concentrations of GGG.

Importantly, deficiency in Abcc1 restored the BM homing ability of P2RY8+ cells (**Fig 2.5a**). While loss of Ggt5 had an unclear effect on the intravascular partitioning of P2RY8+ cells (**Supplementary Fig 2.7f**), Abcc1 deficiency notably abrogated the increased vascular presence of P2RY8+ cells in the BM (**Fig 2.5b**). Abcc1 deficiency also abrogated the smaller intravascular bias of P2RY8+ cells seen in the spleen (**Supplementary Fig 2.7g**).

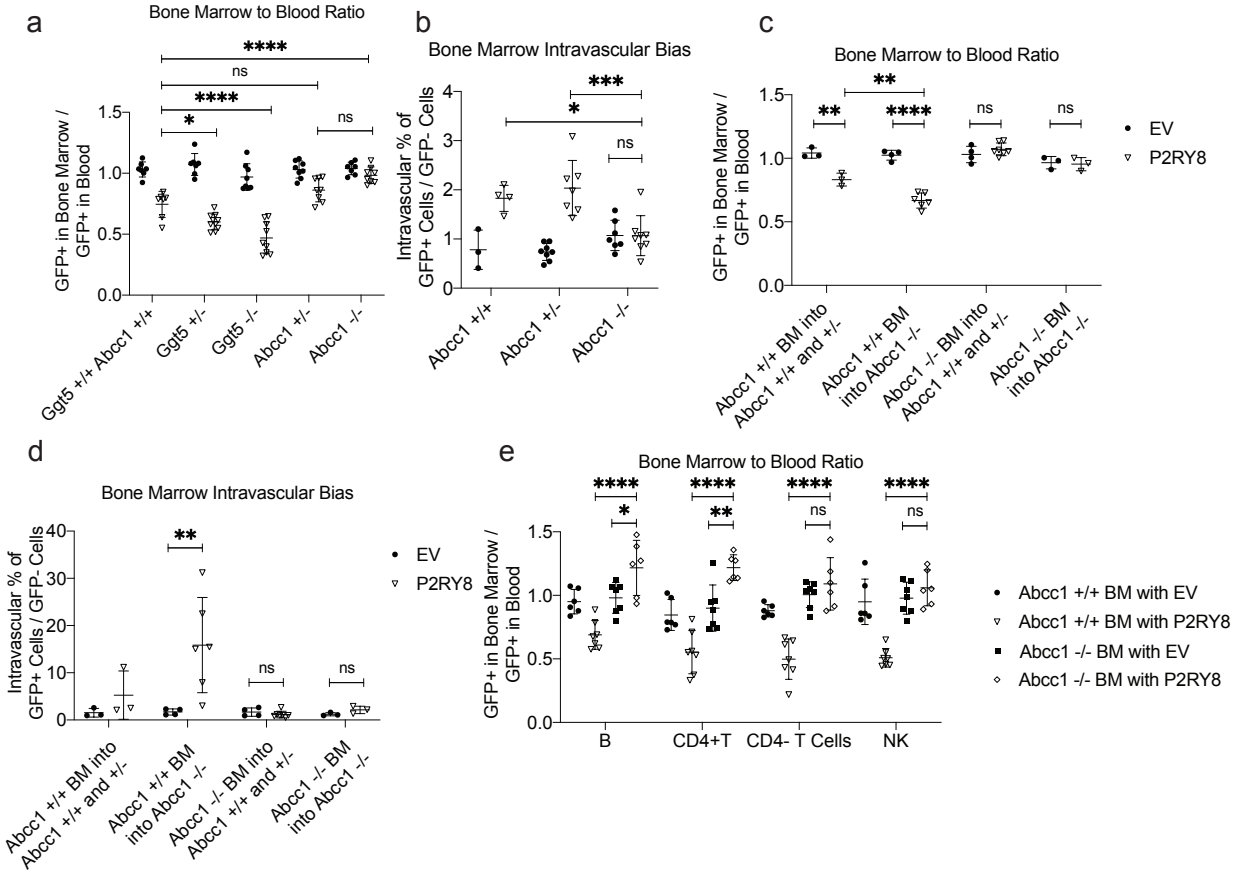

Figure 2.5: Ggt5 and Abcc1 control homing of P2RY8+ lymphocytes to the BM. (a-d) Activated EV- or P2RY8-transduced polyclonal B cells were transferred into preimmunized mice. (a) GFP frequency in the BM divided by GFP frequency in the blood at 24hrs after cell transfer (n=7-10 per group). (b) Percentage of GFP+ cells in each mouse staining with CD45.2-PE injected intravascularly, divided by GFP- cell staining for the same (n= 3-10 per group). (c) GFP frequency in the BM divided by GFP frequency in the blood at 24hrs after cell transfer in Abcc1 chimeric mice. (d) Percentage of GFP+ cells in each individual Abcc1 chimeric mouse staining with CD45.2-PE injected intravascularly, divided by GFP- cell staining for the same (n= 3-7 per group in c,d). (e) GFP+ frequency of mature B, T and NK cells in the BM divided by GFP+ frequency in the blood in congenically marked mice reconstituted with EV- or P2RY8-transduced Abcc1+/+ or -/- BM. Data from Abcc1+/+ BM from this panel is also included in Fig 4d (n=6-7 per group). Data are pooled from seven (a), three (b,c,d), or two (e) experiments. P values determined by one-way ANOVA with Tukey's multiple comparisons test (d). *P<0.05, **P<0.01, ***P<0.001, ****P<0.0001. Graphs depict mean with s.d. and points represent biological replicates.

Given loss of hematopoietic Abcc1 was sufficient to disrupt the P2RY8+ cell localizing behavior in the GC, we aimed to determine if the same was true for the GGG-mediated restriction of cell access to the BM. Thus, we transferred P2RY8+ cells into chimeras reconstituted with the series of combinations of Abcc1 sufficient and deficient BM. The results showed that Abcc1 was required only on hematopoietic cells for the inhibition of P2RY8+ cell migration to the BM (**Fig 2.5c**). Notably, mice lacking Abcc1 in their stromal compartment but retaining Abcc1 in their hematopoietic compartment exhibited an even stronger block in the BM homing of P2RY8+ cells compared to control mice. Moreover, while the intravascular bias of P2RY8+ cells in the BM of these chimeric mice (**Fig 2.5d**) mirrored the phenotype seen at the whole tissue level, the vascular bias seen in mice lacking Abcc1 in just their stromal compartment was on average 15-fold, vs the approximately two-fold bias seen in non-chimeric mice. These data suggest a complexity in the shape of the BM GGG gradient and the cell types contributing to its organization. Abcc1-dependent reduced homing to the BM was not unique to in vitro activated B cells, as mature B cells, CD4+ T cells, CD8+ T cells, and NK cells in mice reconstituted with P2RY8-transduced BM also showed a reduced presence in the BM, which was dependent on Abcc1 (**Fig 2.5e**). Notably, for B cells and CD4+ T cells in this system, there was an increased presence of P2RY8+ cells in the BM of mice lacking Abcc1 in their hematopoietic system. These data suggest that when stromal cells are the only source of extracellular GGG, P2RY8+ cells show enhanced entry into, or reduced exit from, the BM.

Human T cell homing to bone marrow is restricted by P2RY8:

Finally, we sought to test the function of endogenous P2RY8 in human cells in vivo using the NOD-scid-gamma (NSG) mouse model (Lee et al., 2013). Currently there are no well-established protocols for studying human GC formation in humanized mice (Li et al., 2018). However, our finding that P2RY8 expression on mouse lymphocytes leads to decreased homing to the BM gave us the opportunity to test whether endogenous P2RY8 on human cells regulates BM homing in NSG mice. Using CRISPR/Cas9, we ablated P2RY8 in stimulated human CD4 and CD8 T cells isolated from four blood donors. Three days following CRISPR editing, these cells had a confirmed editing efficiency of above 95% by TIDE analysis in three out of four donors (**Fig. 2.6a** and **Supplementary Fig 2.8a,b**), and protein staining of cellular P2RY8 levels via flow cytometry showed decreased staining in both CD4+ and CD8+ edited T cells compared to control cells (**Fig 2.6b**). The edited T cell cultures were tested for their ability to sense GGG during migration to CXCL12, and while control T cells showed partial inhibition in their migration to CXCL12 upon addition of 100 or 1000 nM GGG, P2RY8 KO T cells were not inhibited in their migration (**Fig 2.6c,d** and **Supplementary Fig 2.8c,d**). This finding is notable, as it extends the sites where there is evidence for P2RY8-GGG action in human T cells beyond Tfh cells(Lu et al., 2019), to T cells that have been activated under non-polarizing conditions. Although the degree of migration inhibition is smaller than observed in previous studies for GC B and Tfh cells, it should be noted that in vitro migration assays can be influenced by many parameters (such as cell activation status) and their magnitude often does not equate to the magnitude of the in vivo response. CFSE or CTV labeled P2RY8 KO and control cells were then transferred

intravenously to NSG mice. A time point of 48hrs was chosen to examine T cell homing to the BM in NSG mice as an initial time course experiment showed that human T cells had already significantly accumulated in the BM by this time (**Supplementary Fig 2.8g**). At 48hrs following transfer, P2RY8 KO T cells were more likely to be found in the BM than controls cells, while this representation bias was not seen for cells in the blood (**Fig 2.6e**, **Supplementary Fig 2.8e,f**). This effect was independent of CTV or CFSE labeling (**Supplementary Fig 2.8h**) and correlated with the editing efficiency of each T cell donor culture via TIDE analysis (**Fig 2.6f**). These results indicate that loss of endogenous levels of P2RY8 on human T cells is sufficient to increase homing of these cells to the BM.

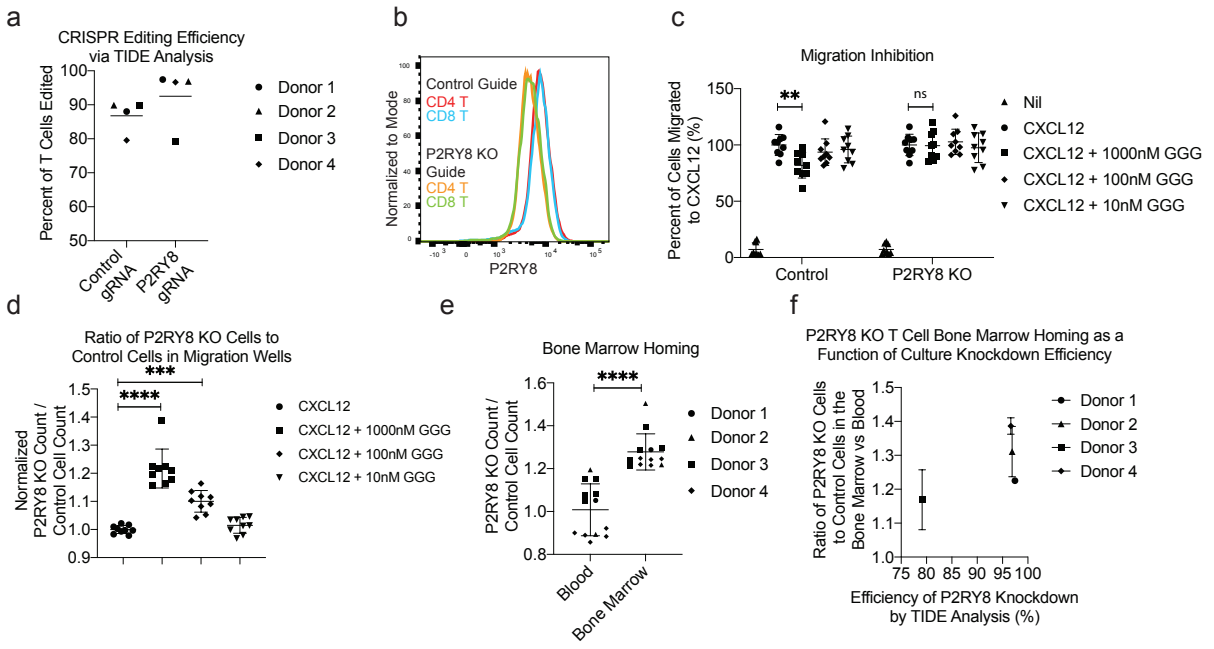

Figure 6: P2RY8 KO Human T cells show elevated BM homing.
Guide RNAs targeting P2RY8 and the AAVS locus (as a control) were used to edit stimulated primary human T cells from 4 donors. (a) TIDE analysis determined CRISPR editing efficiency for each donor. (b) Staining of CRISPR-edited T cells for P2RY8 protein via flow cytometry. (c-f) P2RY8 KO and AAVS KO control T cells from each donor were CFSE and CTV labeled, respectively, and then mixed at a 1:1 ratio. (c-d) Transwell migration assays of the edited cells towards CXCL12 and the indicated concentrations of GGG. (c) Total counts of P2RY8 KO or AAVS KO control cells found to have migrated to the bottom of each transwell, normalized to the count of migrated cells to CXCL12 alone. (d) Ratio of total P2RY8 KO to AAVS KO controls cells in the bottom of each transwell, normalized to the ratio of migrated cells to CXCL12 alone. (e) A 1:1 mix of CFSE+ P2RY8 KO cells and CTV+ AAVS KO control cells was transferred iv into NSG mice. 48hrs later blood and BM was collected and the ratio of P2RY8 KO to AAVS KO control cells in each tissue was assessed. Based on number of edited T cells available, 20 million cells from each donor were transferred into 1-5 NSG mice. (f) BM to blood ratio plotted as a function of CRISPR editing efficiency of the P2RY8 locus for each donor. Data are pooled from four experiments. P values determined by one-way ANOVA with Tukey's multiple comparisons test (d) or unpaired two-tailed Student's t-test (c) or paired two-tailed Student's t-test (e). *P<0.05, **P<0.01, ***P<0.001, ****P<0.0001. Graphs depict mean with s.d. and points represent biological replicates, except in (c) where points represent pooled technical replicates from 4 human donors.

Supplementary Figures and Tables

Supplementary Figure 2.1: Ggt5 is required *in vivo* for P2RY8-mediated follicle center confinement of B cells.

Supplementary Figure 2.2: Abcc1 is required *in vivo* for GGG export.

Supplementary Figure 2.3: Abcc1 expression by B cells is required for P2RY8-mediated follicle center confinement.

Supplementary Figure 2.4: Abcc1 expression by B cells is required for the growth regulation of P2RY8-expressing GC B cells.

Supplementary Figure 2.5: Ggt5 and Abcc1 are not required for the confinement of endogenous mouse GC B cells.

Supplementary Figure 2.6: P2RY8 expression reduces lymphocyte homing to the BM.

Supplementary Figure 2.7: Reduced homing of P2RY8+ B cells into the BM parenchyma, P2RY8, ABCC1, and GGT5 mRNA expression data, and detection of GGG in BM.

Supplementary Figure 2.8: Homing of Human T Cells to the BM of NSG Mice.

Supplementary Table 2.1: Target crRNA sequences and PCR primers.

Supplementary Table 2.2: Antibodies.

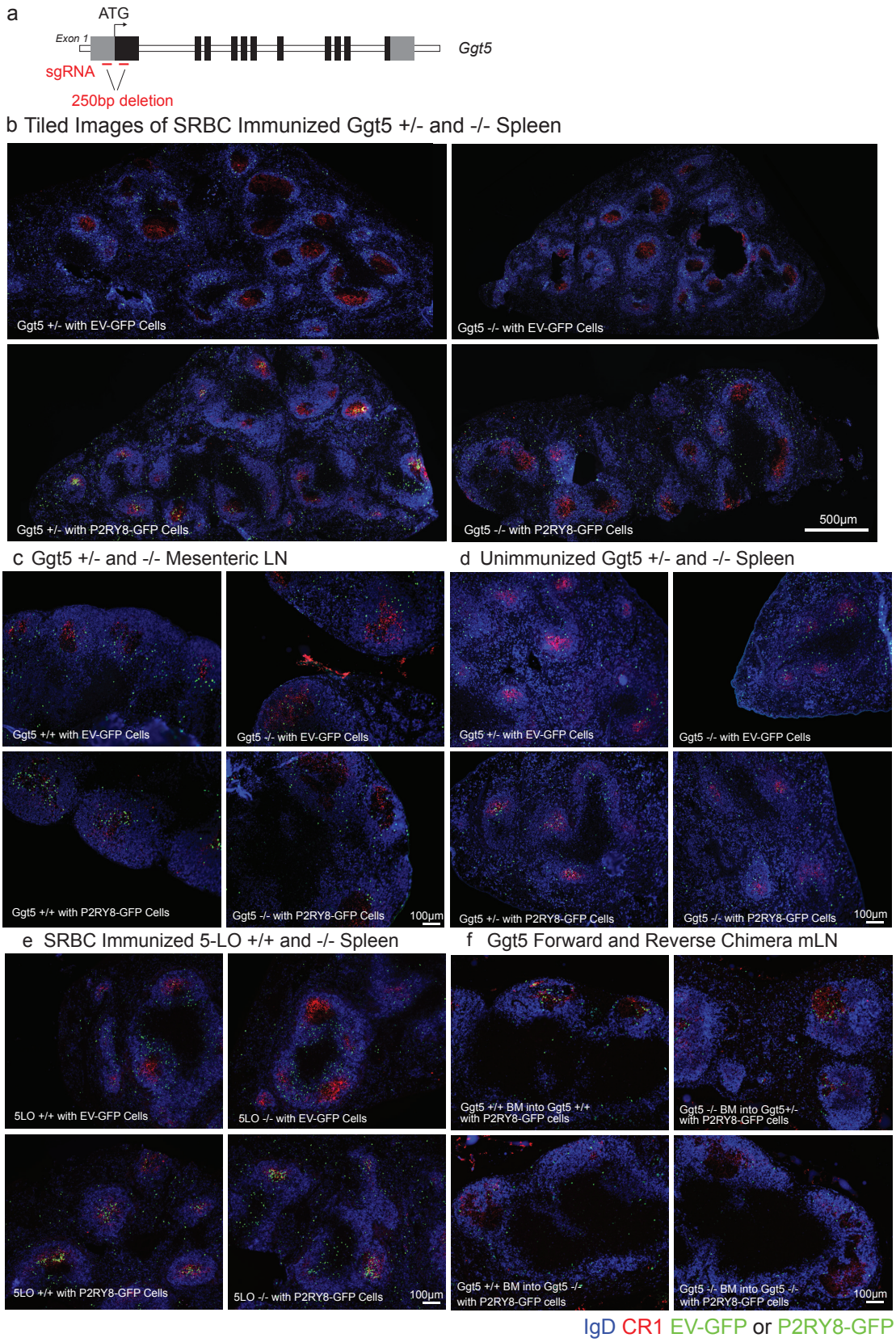
a
ATG
Exon 1
Ggt5
sgRNA
250bp deletion
b Tiled Images of SRBC Immunized Ggt5 +/- and -/- Spleen
Ggt5 +/- with EV-GFP Cells
Ggt5 -/- with EV-GFP Cells
Ggt5 +/- with P2RY8-GFP Cells
Ggt5 -/- with P2RY8-GFP Cells
500µm
c Ggt5 +/- and -/- Mesenteric LN
d Unimmunized Ggt5 +/- and -/- Spleen
Ggt5 +/+ with EV-GFP Cells
Ggt5 -/- with EV-GFP Cells
Ggt5 +/- with EV-GFP Cells
Ggt5 -/- with EV-GFP Cells
Ggt5 +/+ with P2RY8-GFP Cells
Ggt5 -/- with P2RY8-GFP Cells
100µm
Ggt5 +/- with P2RY8-GFP Cells
Ggt5 -/- with P2RY8-GFP Cells
100µm
e SRBC Immunized 5-LO +/+ and -/- Spleen
f Ggt5 Forward and Reverse Chimera mLN
5LO +/+ with EV-GFP Cells
5LO -/- with EV-GFP Cells
Ggt5 +/+ BM into Ggt5 +/+ with P2RY8-GFP cells
Ggt5 -/- BM into Ggt5+/- with P2RY8-GFP cells
5LO +/+ with P2RY8-GFP Cells
5LO -/- with P2RY8-GFP Cells
100µm
Ggt5 +/+ BM into Ggt5 -/- with P2RY8-GFP cells
Ggt5 -/- BM into Ggt5 -/- with P2RY8-GFP cells
100µm
IgD CR1 EV-GFP or P2RY8-GFP

Supplementary Figure 1: Ggt5 is required *in vivo* for P2RY8-mediated follicle center confinement of B cells.
(a) Ggt5 gene organization showing location of sgRNA targeting exon 1 to create a 250bp deletion around the ATG. Sequencing analysis confirmed the deletion. (b-f) Activated EV- or P2RY8-transduced B cells were transferred into mice. (b) Tiled images of full spleen cross sections in SRBC immunized Ggt5 +/- and -/- mice. (c) mLNs of Ggt5 +/- and -/- mice. (d) Spleens of unimmunized Ggt5 +/- and -/- mice. (e) Spleens of SRBC immunized 5-LO +/+ and -/- mice. (f) mLNs of SRBC immunized Ggt5 BM chimeric mice. Immunofluorescence for P2RY8- or EV-transduced B cells (GFP, green) in the FDC-defined region (CR1, red) of mice relative to endogenous follicular B cells (IgD, blue). Scale bar sizes as indicated. Data are representative of six (b), four (c), one (d), three (e) or two (f) biological repeats, with approximately 40 GCs visualized per biological repeat.

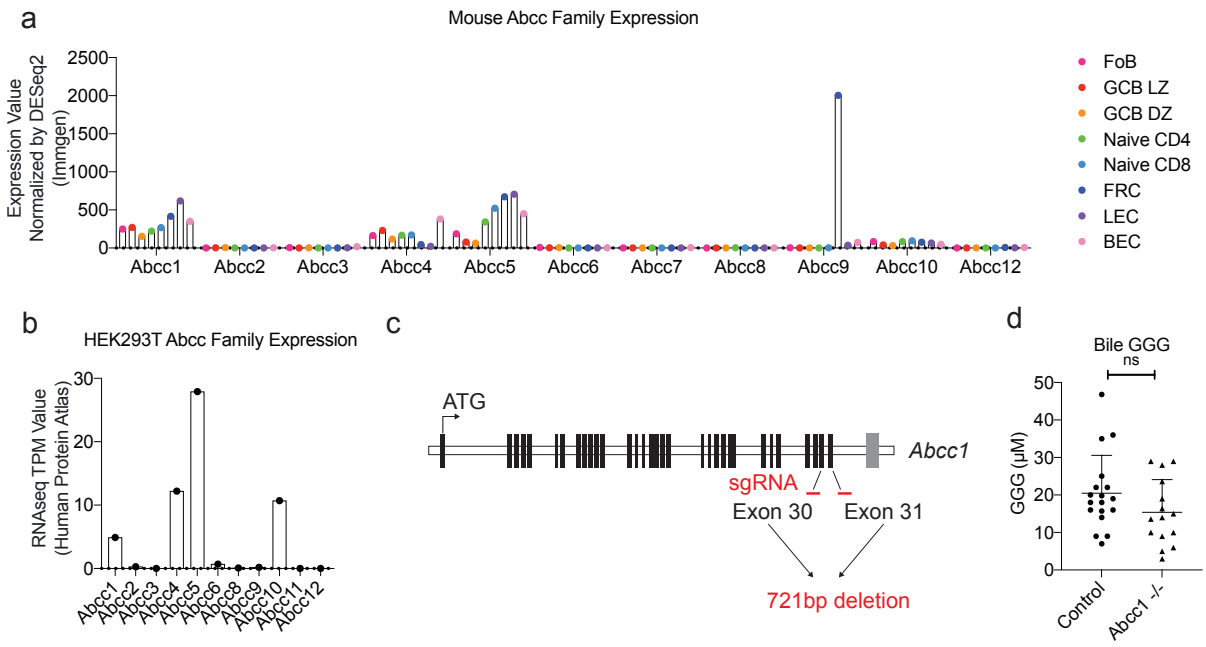

e Tiled Images of SRBC Immunized Abcc1 +/- and -/- Spleen

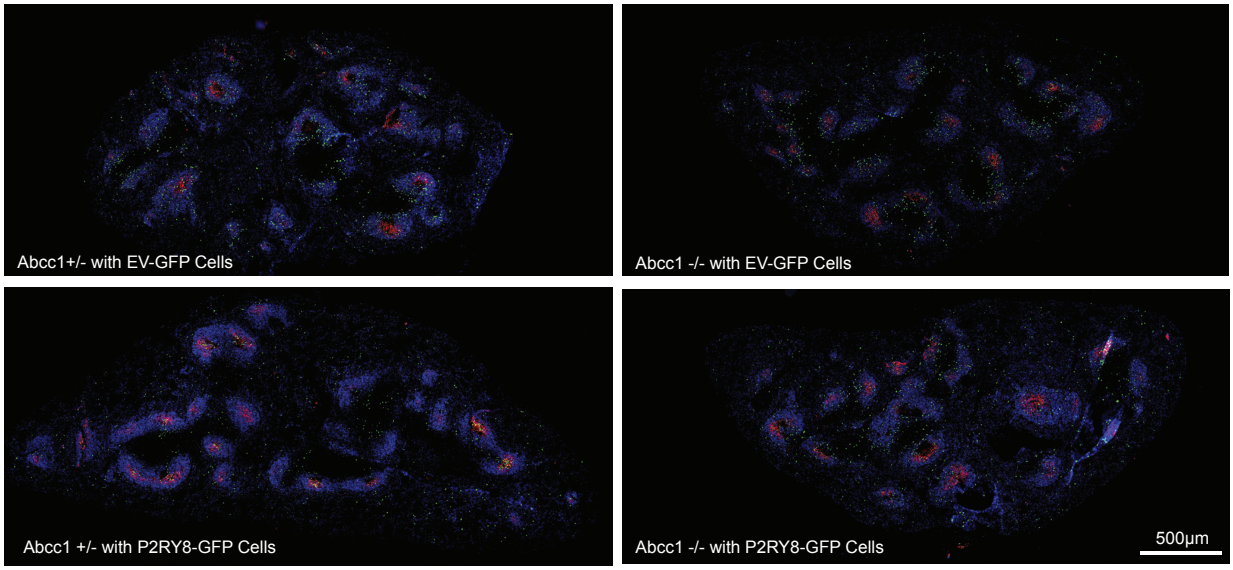

f Abcc1 +/+ and -/- Mesenteric LN

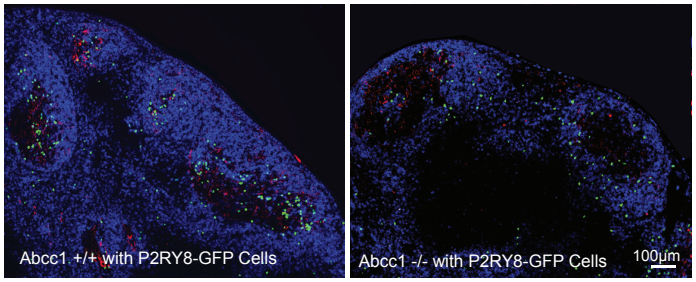

IgD CR1 EV-GFP or P2RY8-GFP

g

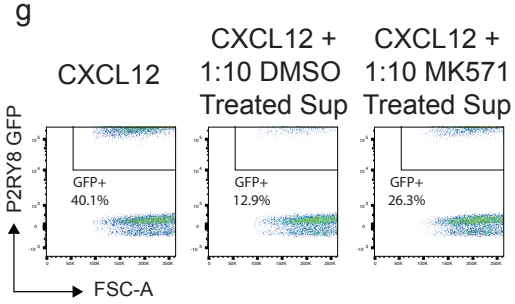

Supplementary Figure 2: Abcc1 is required *in vivo* for GGG export.
(a-b) RNAseq expression data for the Abcc family of transporters in mouse lymphoid tissue cells from Immgen.org (a) and in human HEK293T cells from the Human Protein Atlas (proteinatlas.org) (b). Data were downloaded from proteinatlas.org and compiled using R. (c) Abcc1 gene organization showing location of sgRNA targeting exons 30 and 31 to create a 721bp deletion. Sequencing analysis confirmed the deletion. (d) GGG levels were measured in the bile of Abcc1-/- and control (Abcc1+/+ and +/- littermate controls) via LC-MS/MS (n= 18 control, n=15 Abcc1-/-). (e-f) Activated EV- or P2RY8-transduced B cells were transferred into preimmunized Abcc1 +/+, +/- or -/- mice, and tiled images of full spleen cross sections (e) or mLN (f) are shown. Immunofluorescence for P2RY8- or EV-transduced B cells (GFP, green) in the GCs (CR1, red) of SRBC immunized mice relative to endogenous follicular B cells (IgD, blue). Scale bar sizes as indicated. (g) Example of FACS gating for the identification of P2RY8+ WEHI cell migration to CXCL12 in the presence of supernatant from MK571-treated HEK293T cells. Data are pooled from two experiments (d); or representative of three experiments (g); or representative of four (e) or two (f) biological repeats, with approximately 40 GCs viewed per imaging biological repeat. P values determined by unpaired two-tailed Student's t-test (d). *P<0.05, **P<0.01, ***P<0.001, ****P<0.0001. Graphs in (d) depict mean with s.d. and points represent biological replicates.

a Abcc1 Forward and Reverse Chimera Tiled Images of Spleen- *High Cell Transfer Amount*

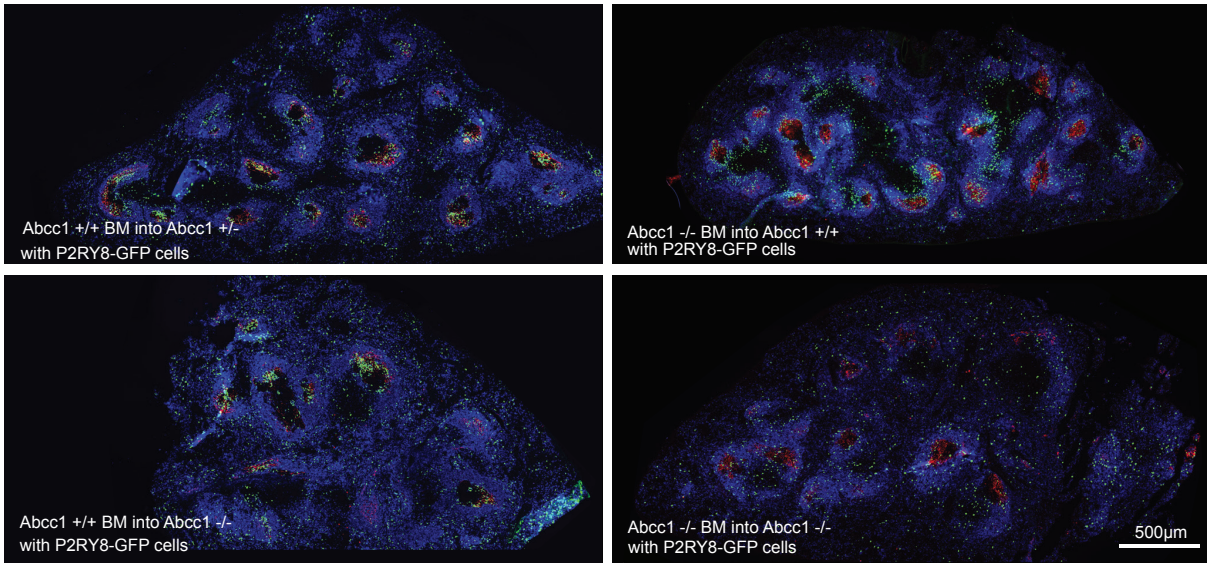

b Abcc1 Forward and Reverse Chimera mLN

c μMT:Abcc1 Mixed Chimera Spleen Images

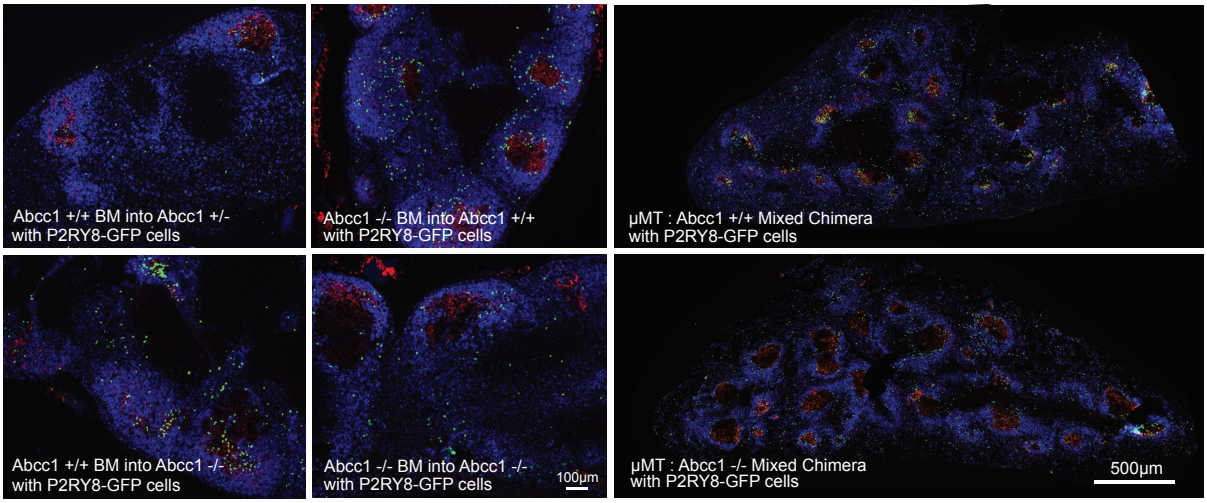

d "Ringing" Behavior in μMT:Abcc1 Mixed Chimera Spleens

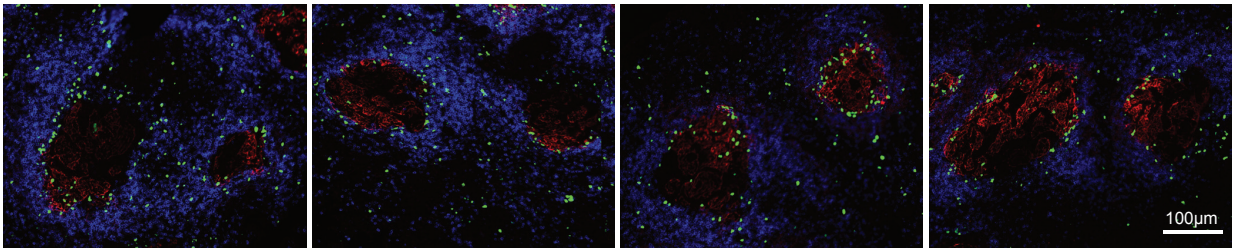

IgD CR1 EV-GFP or P2RY8-GFP

Supplementary Figure 3: Abcc1 expression by B cells is required for P2RY8-mediated follicle center confinement.

(a-c) Activated P2RY8-transduced B cells were transferred into preimmunized mice. (a) Tiled images of full spleen cross sections in Abcc1 BM chimeric mice of the indicated types. Here, approximately twice as many P2RY8+ cells were transferred into each mouse compared to Supplementary Figure 2e. (b) mLN images from Abcc1 chimeric mice. (c) Tiled images of full spleen cross sections in preimmunized Abcc1+/+ mice reconstituted with μMT BM mixed at a 3:1 ratio with Abcc1+/+ or -/- BM. Immunofluorescence for P2RY8- or EV-transduced B cells (GFP, green) in the GCs (CR1, red) of SRBC immunized mice relative to endogenous follicular B cells (IgD, blue). Scale bar sizes as indicated. (d) Additional examples of “ringing” behavior of P2RY8+ cells seen in μMT:Abcc1-/- mixed chimeras. Data in (a,b,c,d) are representative of four biological repeats, with approximately 40 GCs viewed per biological repeat. P values determined by one-way ANOVA with Tukey’s multiple comparisons test (d). *P<0.05, **P<0.01, ***P<0.001, ****P<0.0001. Graphs depict mean with s.d. and points represent biological replicates.

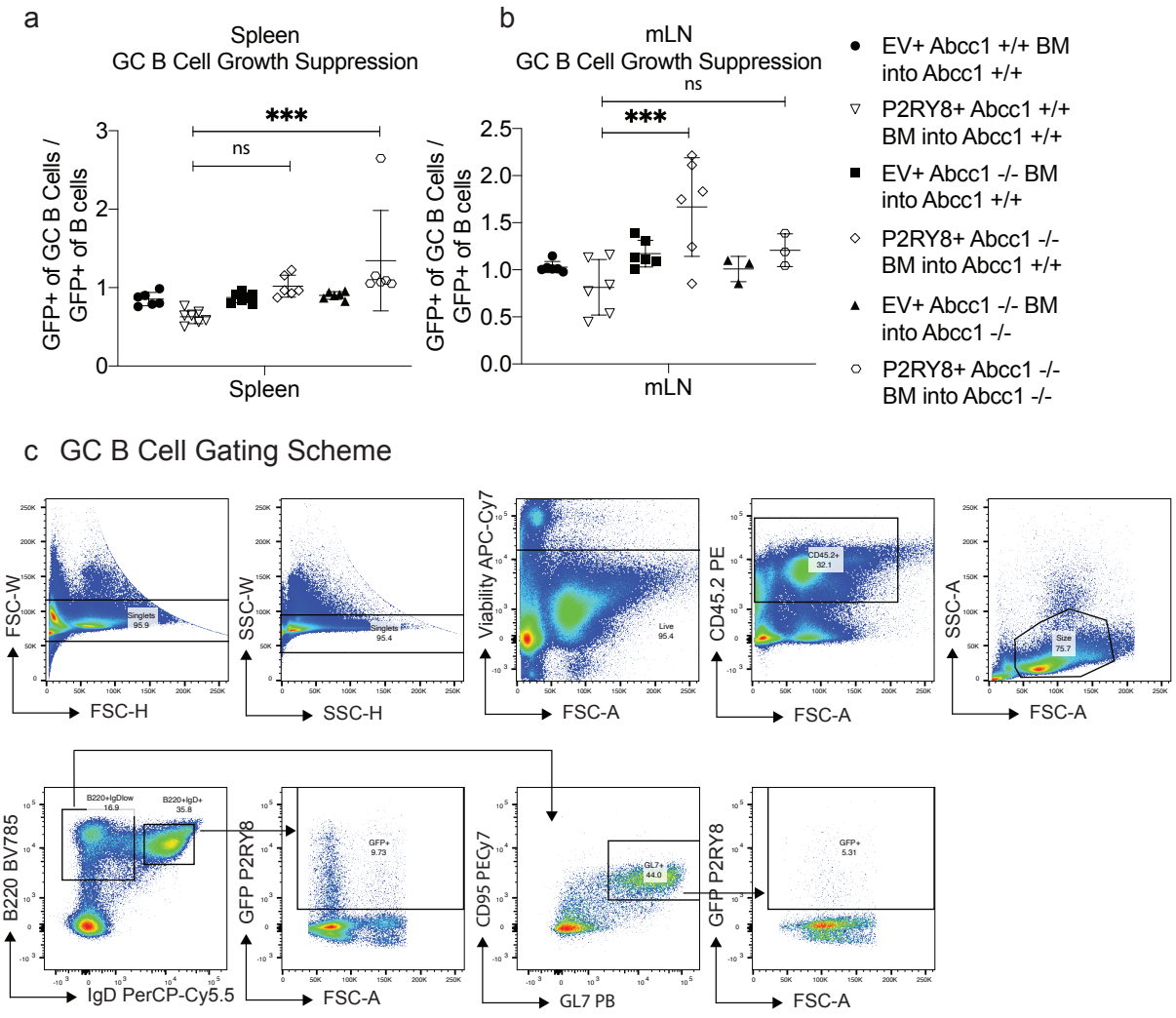

Supplementary Figure 4: Abcc1 expression by B cells is required for the growth regulation of P2RY8-expressing GC B cells.
(a,b) Irradiated Abcc1+/+ or -/- mice were reconstituted with P2RY8-GFP or EV-GFP transduced Abcc1+/+ or -/- BM. (a) Mice were immunized with SRBC and spleens were analyzed for the frequency of GFP+ B cells in the follicular and GC compartment. The ratio of GFP+ cells in the GC B cells vs in the follicular B cells was plotted (n=6 for all but P2RY8+ Abcc1+/+ BM into Abcc1+/+ and EV+ Abcc1-/- BM into Abcc1 -/-, where n=7). (b) mLN were analyzed for the frequency of GFP+ B cells in the follicular and GC compartment in unimmunized mice (n=6 for all but EV+ and P2RY8+ Abcc1-/- BM into Abcc1-/-, where n=3). (c) Example of FACS gating scheme for the identification of GC and follicular B cells in PPs, mLN, spleen and lymph. Data shown for splenic GC B cells of an Abcc1 +/+ mouse that received P2RY8+ Abcc1+/+ BM. Data are pooled from two experiments (a,b). P values determined by one-way ANOVA with Tukey's multiple comparisons test (a,b). *P<0.05, **P<0.01, ***P<0.001, ****P<0.0001. Graphs depict mean with s.d. and points represent biological replicates.

a Confinement of Endogenous Mouse B Cells

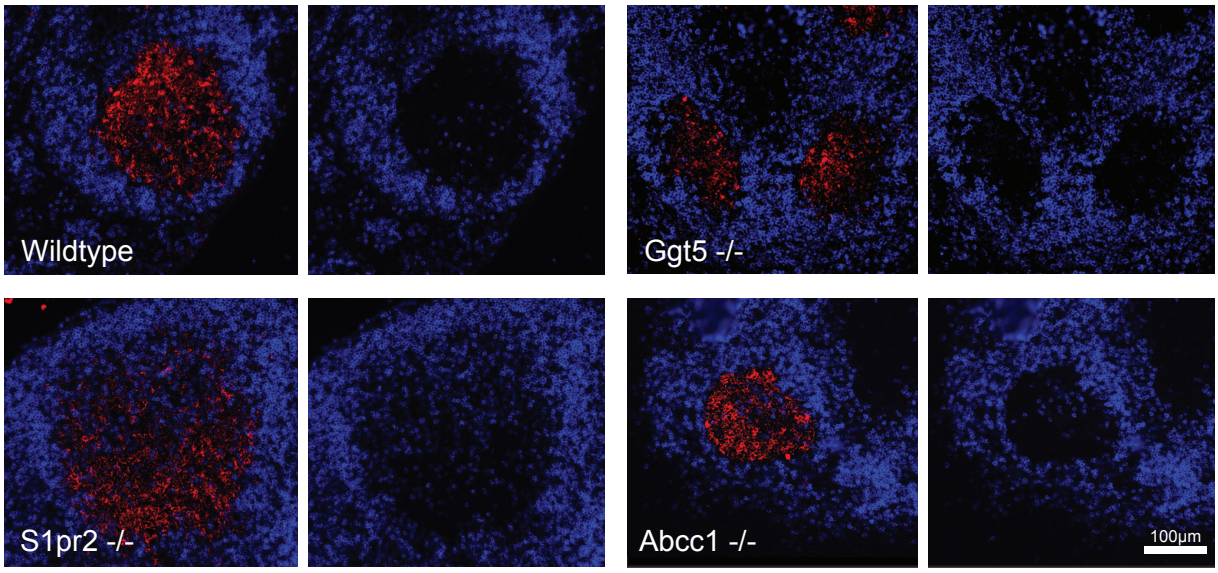

b

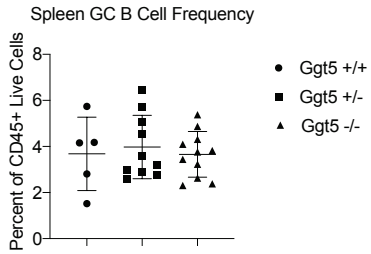

c

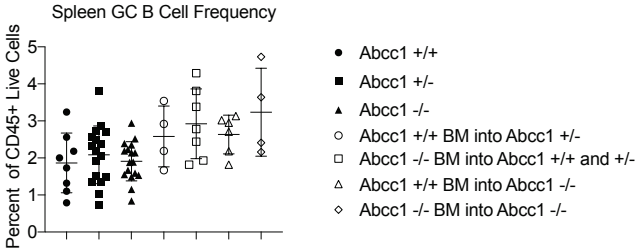

d

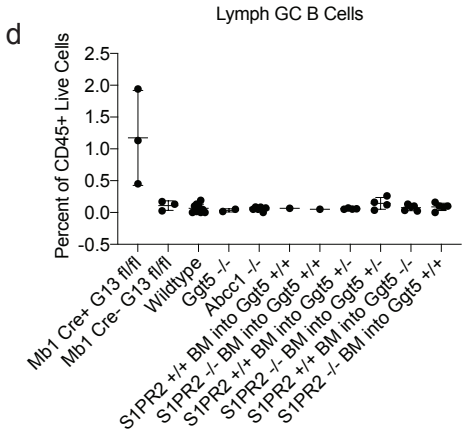

Supplementary Figure 5: Ggt5 and Abcc1 are not required for the confinement of endogenous mouse GC B cells.
(a) Immunofluorescence for GC B cells (GL7, red) in the mLN of SRBC immunized mice relative to endogenous follicular B cells (IgD, blue), showing increased intermixing of IgD+ follicular B cells and GC B cells in S1PR2-/-, but not wildtype, Ggt5-/- or Abcc1-/- mice. Scale bar 100μm. (b-c) Spleen GC B cell frequency at day 6 following SRBC immunization in Ggt5-/- mice (b) and Abcc1-/- mice (c) (n=4-17 per group). (d) GC B cell frequency in lymph collected from the cysterna chyli (n=1-10 per group). Data are pooled from four (b), six (c), or three (d) experiments; or representative of two-six (a) biological repeats, with approximately 10 GCs viewed per biological repeat. Graphs depict mean with s.d. and points represent biological replicates.

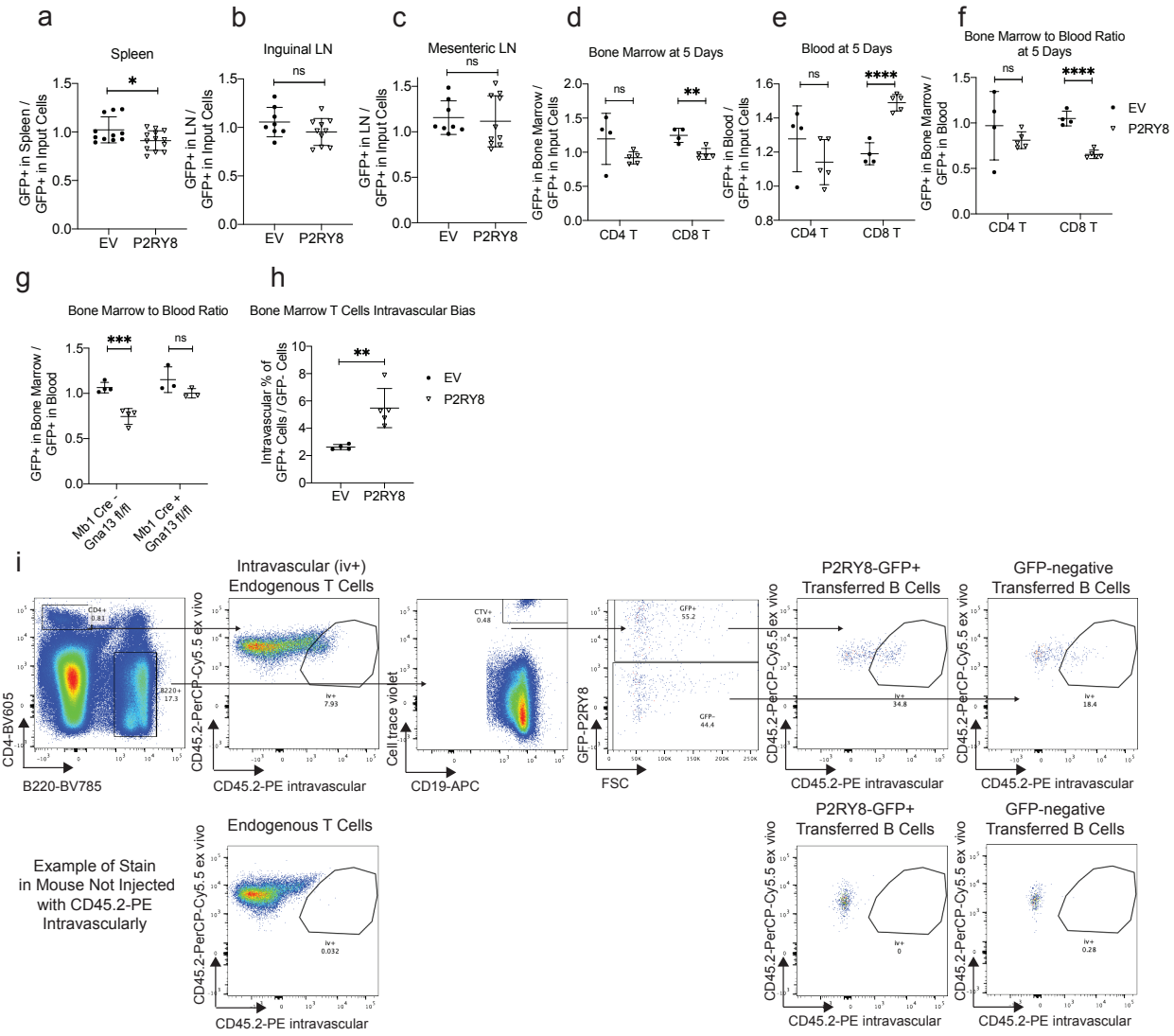
a
Spleen
GFP+ in Spleen / GFP+ in Input Cells
*
EV
P2RY8
b
Inguinal LN
GFP+ in LN / GFP+ in Input Cells
ns
c
Mesenteric LN
GFP+ in LN / GFP+ in Input Cells
ns
d
Bone Marrow at 5 Days
GFP+ in Bone Marrow / GFP+ in Input Cells
ns
**
CD4 T
CD8 T
e
Blood at 5 Days
GFP+ in Blood / GFP+ in Input Cells
ns
****
f
Bone Marrow to Blood Ratio at 5 Days
GFP+ in Bone Marrow / GFP+ in Blood
EV
P2RY8
g
Bone Marrow to Blood Ratio
GFP+ in Bone Marrow / GFP+ in Blood
***
Mb1 Cre - Gna13 fl/fl
Mb1 Cre + Gna13 fl/fl
h
Bone Marrow T Cells Intravascular Bias
Intravascular % of GFP+ Cells / GFP- Cells
**
i
Intravascular (iv+) Endogenous T Cells
CD4-BV605
B220-BV785
CD45.2-PerCP-Cy5.5 ex vivo
CD45.2-PE intravascular
Cell trace violet
CD19-APC
GFP-P2RY8
FSC
P2RY8-GFP+ Transferred B Cells
GFP-negative Transferred B Cells
Example of Stain in Mouse Not Injected with CD45.2-PE Intravascularly
Endogenous T Cells
P2RY8-GFP+ Transferred B Cells
GFP-negative Transferred B Cells

Supplementary Figure 6: P2RY8 expression reduces lymphocyte homing to the BM.

(a-c) Activated EV-or P2RY8-transduced B cells were transferred into preimmunized mice. GFP frequency in the spleen (a), inguinal LN (b), or mLN (c) after 24hrs is plotted as a ratio of the GFP frequency at the time of transfer into mice (n= 11-13 in a, n= 6-8 in b,c). (d-f, h) Activated EV- or P2RY8-transduced polyclonal T cells were transferred into wildtype mice. 5 days after transfer, GFP frequency in the BM (d) or blood (e) is plotted as a ratio of the GFP frequency at the time of transfer into mice. (f) GFP frequency in the BM divided by GFP frequency in the blood at 5 days after cell transfer (n= 4-5 for d,e,f,h). (g) Activated B cells from Mb1 Cre+ and Cre- Gna13 fl/fl mice were transduced with EV or P2RY8 before being transferred into wildtype mice. GFP frequency in the BM divided by GFP frequency in the blood at 24hrs after cell transfer was plotted (n=3-4). (h) At 5 days post transfer, percentage of GFP+ CD8+ T cells in each individual mouse staining with CD45.2-PE injected intravascularly, divided by GFP- CD8+ T cell staining for the same. CD8+ T cells had proliferated after 5 days, preventing pre-gating on CTV-labeled transferred cells. Thus the GFP- values used in this plot reflects all untransduced cells in each mouse, as opposed to just those transferred into the mouse. (i) Example gating scheme for CTV-labeled, transferred GFP+ and GFP- cells, with CD45.2-PE intravascular gating, with gate set by endogenous mouse T cells in the BM. Data are pooled from two (d,e,f,g), three (b,c), or four (a) experiments; or are representative of two (h) experiments. P values determined by unpaired two-tailed Student's t-test. *P<0.05, **P<0.01, ***P<0.001, ****P<0.0001. Graphs depict mean with s.d. and points represent biological replicates.

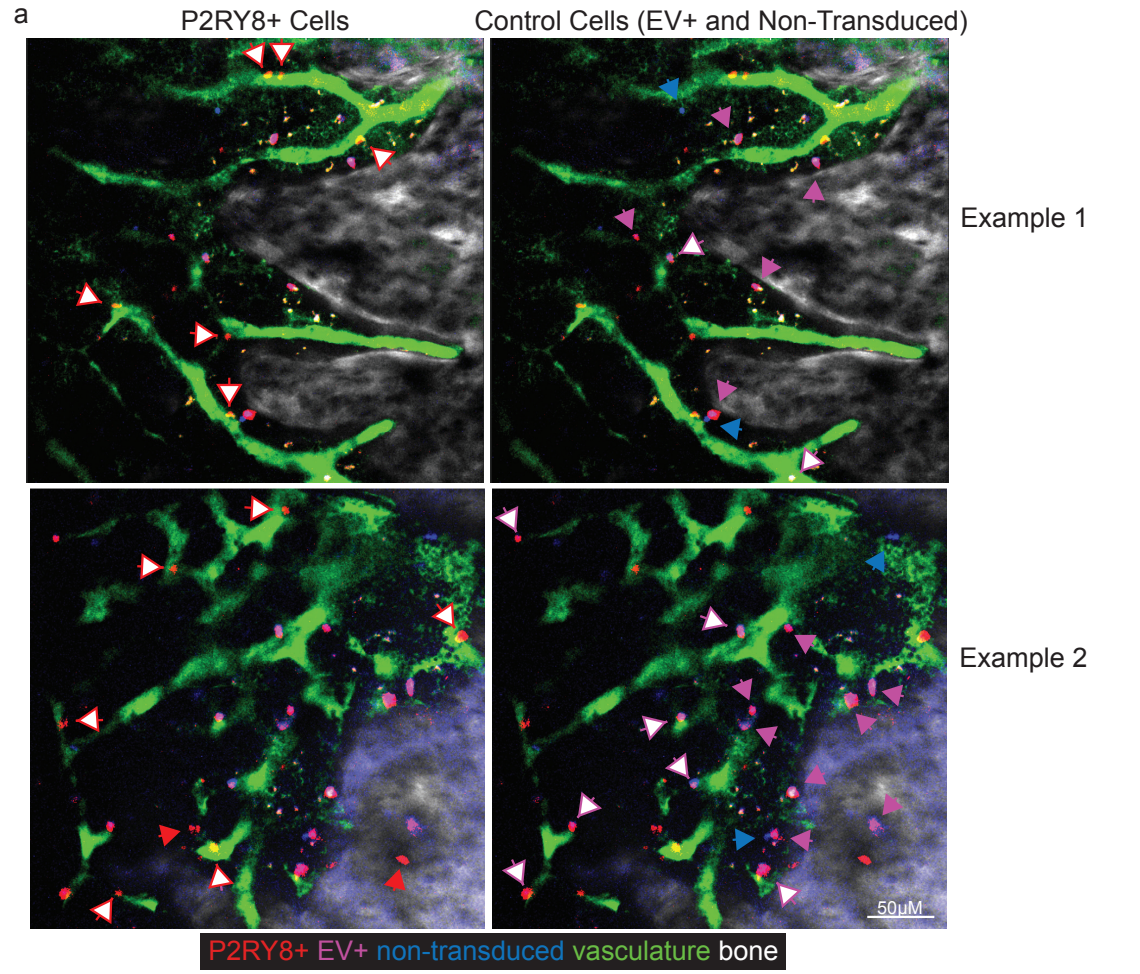
a
P2RY8+ Cells
Control Cells (EV+ and Non-Transduced)
Example 1
Example 2
50μM
P2RY8+ EV+ non-transduced vasculature bone

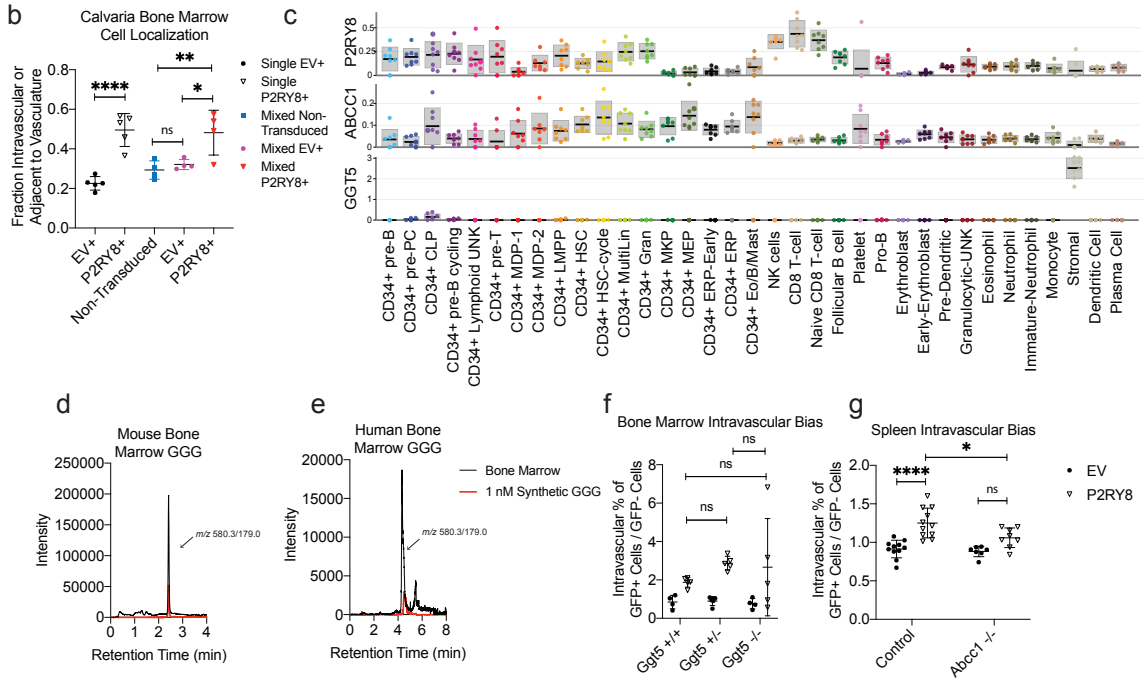
b
Calvaria Bone Marrow Cell Localization
Fraction Intravascular or Adjacent to Vasculature
Single EV+
Single P2RY8+
Mixed Non-Transduced
Mixed EV+
Mixed P2RY8+
EV+
P2RY8+
Non-Transduced
c
P2RY8
ABCC1
GGT5
CD34+ pre-B
CD34+ pre-PC
CD34+ CLP
CD34+ pre-B cycling
CD34+ Lymphoid UNK
CD34+ pre-T
CD34+ MDP-1
CD34+ MDP-2
CD34+ LMPP
CD34+ HSC
CD34+ HSC-cycle
CD34+ MultiLin
CD34+ Gran
CD34+ MKP
CD34+ MEP
CD34+ ERP-Early
CD34+ ERP
CD34+ Eo/B/Mast
NK cells
CD8 T-cell
Naive CD8 T-cell
Follicular B cell
Platelet
Pro-B
Erythroblast
Early-Erythroblast
Pre-Dendritic
Granulocytic-UNK
Eosinophil
Neutrophil
Immature-Neutrophil
Monocyte
Stromal
Dendritic Cell
Plasma Cell
d
Mouse Bone Marrow GGG
Intensity
m/z 580.3/179.0
Retention Time (min)
e
Human Bone Marrow GGG
Bone Marrow
1 nM Synthetic GGG
Intensity
m/z 580.3/179.0
Retention Time (min)
f
Bone Marrow Intravascular Bias
Intravascular % of GFP+ Cells / GFP- Cells
Ggt5 +/+
Ggt5 +/-
Ggt5 -/-
g
Spleen Intravascular Bias
Intravascular % of GFP+ Cells / GFP- Cells
Control
Abcc1 -/-
EV
P2RY8

Supplementary Figure 7: Reduced homing of P2RY8+ B cells into the BM parenchyma, P2RY8, ABCC1 and GGT5 mRNA expression data, and detection of GGG in BM.

(a,b) Two example images and quantification of the corresponding data set demonstrating the localization of a total of 4,289 EV+ and P2RY8+ B cells in the BM. (a) Activated B cells from an EV-GFP transduced culture were labeled with CTV and mixed with P2RY8-GFP transduced B cells such that EV-GFP and P2RY8-GFP were present at a 1:1 ratio. Cells were injected iv into mice and 24 hrs later the BM of the calvaria was imaged by two photon microscopy in euthanized mice in which the vasculature was labeled via injection of fluorescent dextran. Vasculature shown in green, GFP in red, CTV in blue, and second harmonics in white. Red cells represent P2RY8-transduced cells, pink cells represent EV-transduced cells, blue cells represent non-transduced cells from the EV culture, and punctate yellow/white staining represents autofluorescent cells of the marrow. Arrow heads highlight P2RY8 cells of the corresponding color in the left panels, and control cells of the corresponding color in the right panel. Open arrows identify vasculature associated cells and filled arrows identify parenchyma residing cells. (b) Percentage of EV+ and P2RY8+ cells associated with the vasculature of the BM, as quantified from two photon microscopy images . Data are from 4 “mixed” transfer experiments as described in (a), and from 5 “single” transfer experiments in which EV+ and P2RY8+ cells were transferred into separate animals. (c) P2RY8, ABCC1 and GGT5 expression data from the Human Cell Atlas single cell BM sequencing. (d,e) LC-MS/MS chromatograms of 1 nM synthetic GGG (red) overlayed with mouse BM GGG (d) and human BM aspirate GGG (e), calculated from m/z 580.3/179.0 [M+H]+. The difference in retention time reflects the use of different LC-MS instruments for the mouse and human analysis. (f,g) Percentage of GFP+ cells in each individual mouse staining with CD45.2-PE injected intravascularly, divided by GFP- cell staining for the same. (f) BM (n=4-5) and (g) spleen (n=7-11), where control is pooled Abcc1+/+ and +/- mice. Data are pooled from three (g), five (f) or nine (b) experiments; or are representative of five (a,d,e) experiments. P values determined by one-way ANOVA with Tukey’s multiple comparisons test (b,f,g). *P<0.05, **P<0.01, ***P<0.001, ****P<0.0001. Graphs depict mean with s.d. and points represent biological replicates.

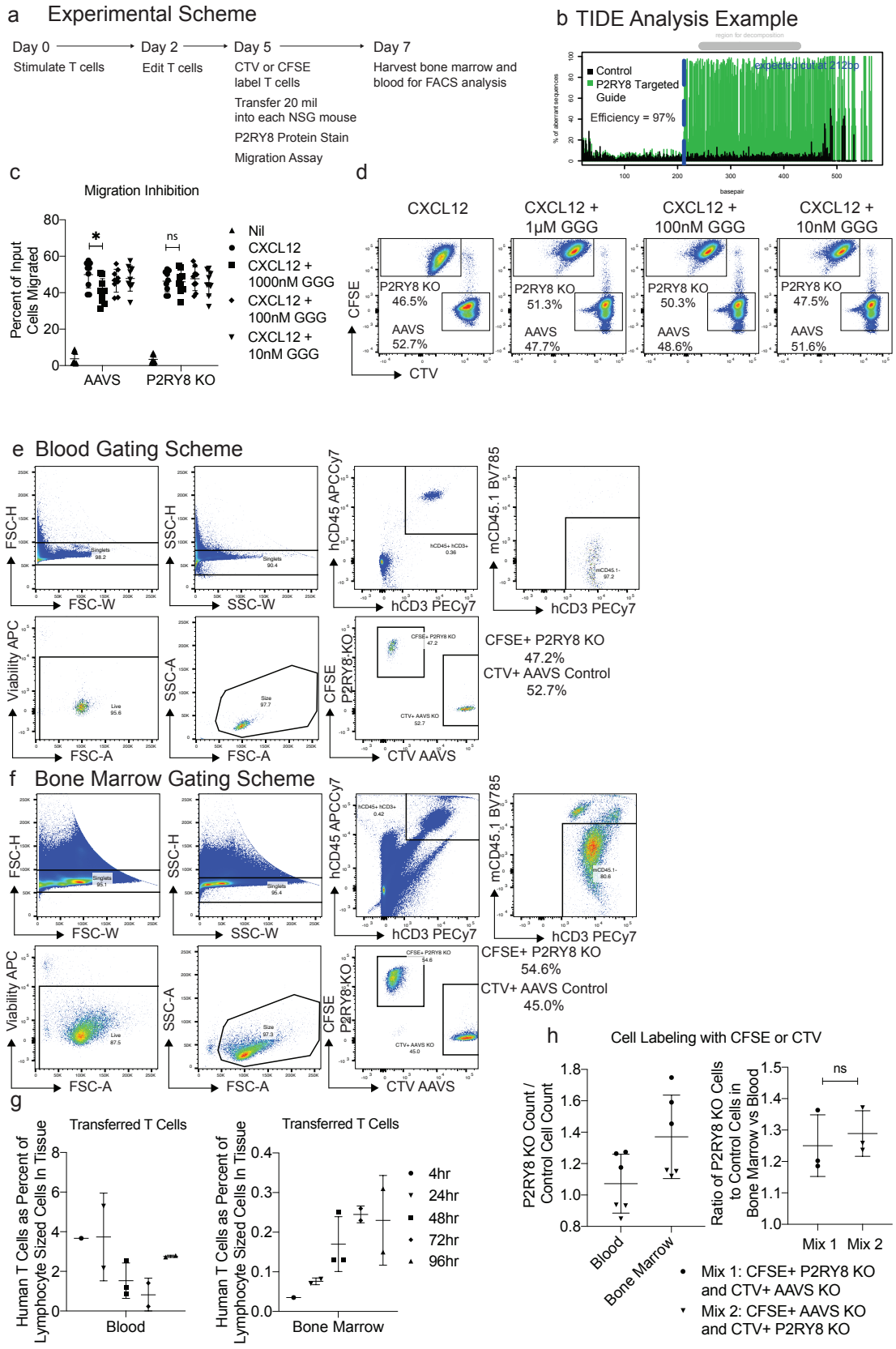
a Experimental Scheme
Day 0
Stimulate T cells
Day 2
Edit T cells
Day 5
CTV or CFSE label T cells
Transfer 20 mil into each NSG mouse
P2RY8 Protein Stain
Migration Assay
Day 7
Harvest bone marrow and blood for FACS analysis
b TIDE Analysis Example
Control
P2RY8 Targeted Guide
Efficiency = 97%
% of aberrant sequences
basepair
c
Migration Inhibition
Percent of Input Cells Migrated
AAVS
P2RY8 KO
Nil
CXCL12
CXCL12 + 1000nM GGG
CXCL12 + 100nM GGG
CXCL12 + 10nM GGG
d
CXCL12
CXCL12 + 1μM GGG
CXCL12 + 100nM GGG
CXCL12 + 10nM GGG
CFSE
CTV
P2RY8 KO 46.5%
AAVS 52.7%
P2RY8 KO 51.3%
AAVS 47.7%
P2RY8 KO 50.3%
AAVS 48.6%
P2RY8 KO 47.5%
AAVS 51.6%
e Blood Gating Scheme
FSC-H
FSC-W
SSC-H
SSC-W
hCD45 APCCy7
hCD3 PECy7
mCD45.1 BV785
Viability APC
FSC-A
SSC-A
CFSE P2RY8 KO
CTV AAVS
CFSE+ P2RY8 KO 47.2%
CTV+ AAVS Control 52.7%
f Bone Marrow Gating Scheme
CFSE+ P2RY8 KO 54.6%
CTV+ AAVS Control 45.0%
g
Transferred T Cells
Human T Cells as Percent of Lymphocyte Sized Cells In Tissue
Blood
Bone Marrow
4hr
24hr
48hr
72hr
96hr
h
Cell Labeling with CFSE or CTV
P2RY8 KO Count / Control Cell Count
Ratio of P2RY8 KO Cells to Control Cells in Bone Marrow vs Blood
ns
Mix 1
Mix 2
Mix 1: CFSE+ P2RY8 KO and CTV+ AAVS KO
Mix 2: CFSE+ AAVS KO and CTV+ P2RY8 KO

Supplementary Figure 8: Homing of Human T Cells to the BM of NSG Mice.

(a) Experimental scheme for CRISPR-editing of human T cells and transfer into NSG mice. (b) TIDE analysis of P2RY8-edited vs non-edited control T cells showing editing efficiency around the expected cut site. (c) Transwell migration assays of the edited cells towards CXCL12 and the indicated concentrations of GGG. Total counts of P2RY8 KO or AAVS KO control cells found to have migrated to the bottom of each transwell, as a percent of total cells input into the transwell at the start of the migration experiment. (d) Representative FACS plots from the migration assays showing the collected cells from beneath the transwells for the four conditions listed. (e,f) Example of FACS gating scheme for the identification of P2RY8 KO and AAVS KO human T cells in NSG mouse blood (e) and BM (f). (g) Time course of human T cell frequency in the blood and BM of NSG mice. (h) Flipped CFSE and CTV labeling of P2RY8 KO cells and AAVS KO cells. The absolute count of P2RY8 KO cells was divided by the count of AAVS KO cells in the BM and the blood, and this ratio is shown in the left plot. The resulting ratio in the BM was divided by the ratio in the blood, and this secondary ratio is shown in the right plot, demonstrating equal BM retention of P2RY8 KO cells independent of CFSE or CTV labeling. Data are pooled from two experiments in (g), and representative of one experiment in (h). P values determined by unpaired two-tailed Student's t-test. *P<0.05, **P<0.01, ***P<0.001, ****P<0.0001. Graphs depict mean with s.d. and points represent biological replicates.

Supplementary Table 2.1: Target crRNA sequences and PCR primers.

Human T Cell Editing						
Gene / Locus	**Target**	**crRNA target sequence**	**PCR Primer 1**	**PCR Primer 2**	**Sequencing Primer 1**	**Sequencing Primer 2**
AAVS1	AAVS1_1	GTCACCAATCCTGTCCCTAG	AGCCACCTCTCCATCCTCTT	CTCCCTCCCAGGATCCTCTC	AGCCACCTCTCCATCCTCTT	CTCCCTCCCAGGATCCTCTC
AAVS1	AAVS1_2	GGGGCCACTAGGGACAGGAT	AGCCACCTCTCCATCCTCTT	CTCCCTCCCAGGATCCTCTC	AGCCACCTCTCCATCCTCTT	CTCCCTCCCAGGATCCTCTC
P2RY8	Exon 2	GCAGCACCCCGAATACCCAG	CTTCCCTCCTTCCCTTGCAG	ACTTGAGGACGTCGAAGCAG	GACAACGCGACGCTGCAGAT	TGGAGCTGAGCGGGTACAGG
Knockout Mouse Line Generation						
Gene / Locus	**Target**	**crRNA target sequence 1**	**crRNA target sequence 2**			
Ggt5	Exon 1	GGGAGGCAACTGGACACACA	AGATCTGCTCGGATATTGGA			
Abcc1	Exon 30-31	AAAGATTCTAGTGTTGGACG	CATATCCAATGAGGACTGCA			

Supplementary Table 2.2: Antibodies.

Reactivity	Antigen	Channel	Company	Catalogue Number
Mouse	CD45.1	BV785	Biolegend	110743
Mouse	CD45.1	PB	Biolegend	110772
Mouse	CD45.2	BV605	Biolegend	109841
Mouse	CD45.2	PERCP-CY5.5	Tonbo Bio	65-0454-U100
Mouse	CD45.2	PE-Cy7	Biolegend	109830
Mouse	CD45.2	PE	Biolegend	109808
Mouse	CD16/32	Unconjugated	Bio X Cell	BE0307
Mouse	CD8a	AF647	Biolegend	100724
Mouse	CD19	APC	Tonbo Bio	20-0193-U100
Mouse	CD35 / CR1	Biotin	BD Biosciences	553816
Mouse	CD86	AF647	Biolegend	105020
Mouse	CD95	PE-Cy7	Fisher	557653
Mouse	CXCR4	Biotin	Fisher	551968
Mouse	IgD	PerCP-CY5.5	Biolegend	405710
Mouse	IgD	AF647	Biolegend	405708
Mouse	NK1.1	APC	Fisher	17-5941-82
Mouse	GL7	PB	Biolegend	144614
Mouse	GL7	Biotin	Thermofisher	13-5902-81
Mouse	TCRb	PerCP-CY5.5	Tonbo Bio	65-5961-U100
Mouse	Fc Block		BD	553142
Human/Mouse	B220	PE-Cy7	Tonbo Bio	60-0452-U100
Human/Mouse	B220	BV785	Biolegend	103246
Human	CD45	APC-Cy7	Fisher	BDB557833
Human	CD3	PE-Cy7	Biolegend	300420
Human	P2RY8	Unconjugated	Sigma	HPA003631-100UL
Human	CD4	PE	Fisher	12-0049-42
Rabbit	Anti-rabbit IgG (H+L), F(ab')2 Fragment	AF647	CST	4414S
	GFP	AF488	Thermofisher	A21311
	Fixable Viability Dye	eFluor 660	eBioscience	65-0864-14
	Fixable Viability Dye	eFluor 780	eBioscience	65-0865-18
	Streptavidin	AF555	Life Technologies	S-21381
	Streptavidin	BV605	Biolegend	405229

Materials and Methods

Study Design

The aim of this study was to characterize the enzymatic and transporter requirements for P2RY8-dependent positioning of B cells in GCs. In the course of our studies, we discovered a function for P2RY8 in restraining lymphocyte homing to the BM. Most of the experiments consisted of enumeration of population frequencies by flow cytometry, assessment of cell distribution using immunofluorescence, and quantitation of GGG abundance using a cell migration-based bioassay or LC-MS/MS. Littermate comparisons were used for all mouse studies unless otherwise indicated. Control and experimental treatments were administered to age- and sex-matched mice that had been allocated to groups randomly, with sample sizes chosen based on previous experience and available co-caged littermates to obtain reproducible results. The investigators were not blinded, with the exception of certain two photon imaging analysis. Experimental replication is indicated in the figure legends. No data was excluded from analysis with one exception: a single mouse failed to reconstitute with transduced BM following irradiation and was thus excluded from the analysis depicted in **Figure 2.3d** and **2.5e**.

Mice

Mice were bred in an internal colony and 6-12-week-old mice of both sexes were used. Ggt5 and Abcc1 lines were internally generated and bred. μMT mice (B6.129S2-Ighmtm1Cgn/J) were obtained from C. Allen at UCSF, and Nod scid gamma (NSG) mice (NOD.Cg-Prkdcscid Il2rgtm1Wjl/SzJ) were obtained from A. Marson and Q. Tang

at UCSF. CD45.1 B6 mice (B6.SJL-PtprcaPepcb/BoyCrCrl) mice were bred internally from founders ordered from JAX, or were purchased from National Cancer Institute at Charles River at age 6–8 wks. Littermate controls were used for experiments, mice were allocated to control and experimental groups randomly, and sample sizes were chosen based on previous experience and available co-caged littermates to obtain reproducible results. Animals were housed in a pathogen-free environment in the Laboratory Animal Resource Center at UCSF, and all experiments conformed to ethical principles and guidelines that were approved by the Institutional Animal Care and Use Committee.

Generation of Ggt5-/- and Abcc1-/- mice

Ggt5-/- mice were generated on the C57BL/6J background using two sgRNAs flanking the exon 1 region deleted in a previously reported Ggt5-deficient mouse strain (Shi et al., 2001) (this line was no longer available as the originating lab had closed). Using CRISPR-EZ we generated a mouse with a 250bp mutation around the ATG, mirroring that found in the original knockout line. Sequencing analysis confirmed the deletion, and also identified frameshift-inducing point mutations at the sgRNA target sites in a second mouse. Both of these mice were crossed to C57B6/J for several generations, and initial phenotypes were tested in both lines. Both lines behaved identically, and the 250bp deletion line was selected to be used as the dominant line.

Abcc1-/- mice were produced on the C57BL/6J background using CRISPR-EZ to generate a deletion spanning exon 30-31, a deletion chosen for its removal of the B-

motif of the second ATP-binding domain, a characteristic domain of this protein family and the same region that was deleted in a previously characterized Abcc1-deficient mouse line (Lorico et al., 1997). Multiple founder mice were generated with deletions ranging from 721-778bp (in comparison to the original 0.7kb deletion). Three of these mice were crossed to C57B6/J for several generations and initial phenotypes were tested in all three lines. Data shown in the figures are from all three lines, as they were functionally identical in all assays tested.

Supplementary Table 2.1 lists the crRNAs used in the generation of Ggt5-/- and Abcc1-/- animals.

The protocol introduced the sgRNAs into B6/J zygotes along with Cas9 mRNA using electroporation (CRISPR-EZ), following the protocol by Chen et al. (Chen et al., 2016), with the main exception that the standard square curve electroporation was performed twice with an interval of 3 s. RNP assembly followed standard protocol: 160 mM tracrRNA + 160 mM crRNA (Dharmacon), equal volume mix well 37˚C, 30 min (80 mM sgRNA); 80 mM sgRNA + 40 mM Cas9 protein equal volume mix well 37˚C 10 min (20 mM RNPs); leave on ice, each electroporation 10 mL of RNPs mix with 10 mL Opti-MEM with C57B6/J embryos. Standard electroporation: two pulses 30V for 3 ms interval 100 ms. Embryos were transferred into pseudo-pregnant females.

Bone marrow chimeras

CD45.1 B6 mice, Ggt5-/- or Abcc1-/- mice where indicated, were lethally irradiated with 1,100 rads gamma-irradiation (split dose separated by 3 h) and then i.v. injected with relevant BM cells.

Mice to be used as BM donors (C57BL/6J, Abcc1+/+ or Abcc1-/- mice) were injected intravenously with 3 mg 5-fluorouracil (Sigma). BM was collected after 4 days and cultured in DMEM containing 15% (v/v) FBS, antibiotics (penicillin (50 IU/ml) and streptomycin (50 mg/ml); Cellgro) and 10 mM HEPES, pH 7.2 (Cellgro), supplemented with IL-3, IL-6 and stem cell factor (at concentrations of 20, 50 or 100 ng/ml, respectively; Peprotech). Cells were 'spin-infected' twice at days 1 and 2 with viral supernatant (MSCV-EV-GFP and MSCV-P2RY8-GFP) and transferred into irradiated CD45.1 B6 recipient mice on day 3. The transduction efficiency of EV and P2RY8 transduced BM cultures was found to be similar, with a mean and standard deviation of 40.04±17.51% for EV and 39.49±11.86% for P2RY8.

Retroviral transduction and activation of lymphocytes

P2RY8 was cloned into the murine stem cell virus MSCV-GFP retroviral vector (P2RY8-GFP) as previously described (Lu et al., 2019). Retrovirus encoding MSCV-P2RY8-GFP and MSCV-EV-GFP was produced using the Platinum-E packaging cell line.

EasySep kits were used to enrich B cells from mouse spleens by removing T cells with biotin-conjugated anti-CD3ε (Biolegend, clone 145-2C11) and streptavidin-conjugated

beads (EasySep Streptavidin RapidSpheres). B cells were cultured in 6-well plates with a final concentration of 0.25 μg/ml (1:4,000 dilution) anti-CD180 (BD Biosciences, clone RP/14), diluted in RPMI 1640 containing 10% FBS, 10 mM HEPES, 55 μM 2-mercaptoethanol, 2 mM glutamine and 50 IU penicillin/streptomycin.

For transduction of polyclonal T cells, 24 well plates were coated with 300μl per well of LEAF-purified anti-CD3 (Biolegend, clone 145-2C11) at 3μg/ml and anti-CD28 (Biolegend, Clone 37.51) at 0.5μg/ml overnight. The next day wildtype polyclonal T cells were isolated from peripheral LNs, mesenteric LNs, and spleens and enriched using EasySep kits to remove B cells (anti-B220-biotin from Tonbo Bio and EasySep Streptavidin RapidSpheres). Plates were washed with PBS, and then T cells were plated at 1 mil T cells per well in RPMI 1640 containing 10% FBS, 10 mM HEPES, 55 μM 2-mercaptoethanol, 2 mM glutamine and 50 IU penicillin/streptomycin. 24 hrs after activation of B cells and T cells, the plates were centrifuged and the culture supernatant was saved. HEPES and polybrene (EMD Millipore) were added to the retrovirus to a concentration of 20mM and 2μg/ml, respectively. This retroviral medium was used to spinfect the cells at 2,500 r.p.m. for 2 hr at room temperature, the viral supernatant was aspirated and the original culture supernatant was returned to the cells. This spinfection was repeated for a second time, 24 hr later. Twenty-four hours after the second spinfection, cells were collected from each plate and washed twice. Cells were labeled with Cell Trace Violet (Fisher), counted, and adoptively transferred into immunized mice on day 6 after immunization with SRBCs. 5-7 mil GFP+ B cells (“Low transfer amount”), or 10-14 mil GFP+ B cells (“High transfer amount”), were transferred when spleen or LN

follicle localizing behavior was being tested to ensure adequate numbers of cells could be viewed by immunofluorescence. At least 2 mil GFP+ B cells or T cells were transferred when homing was being tested. Up to 60 mil GFP+ cells were transferred when homing to the BM was being evaluated with two photon microscopy. Mice were analyzed 24 hr after transfer for all experiments, except for when T cell BM homing was examined 5 days following transfer. Transduced B cells comprised 1–3% (GFP) of all B cells in the spleen by flow cytometry when 5-7 mil GFP+ B cells were transferred. Homing of GFP+ cells was tracking by flow cytometry and positioning of GFP-expressing B cells was tracked by immunofluorescence or two photon microscopy.

To measure the export of GGG by polyclonal B cells in vitro, splenic B cells were activated with anti-CD180 as described. 72 hrs after activation, supernatants were collected.

Immunofluorescence

Spleens were fixed in 4% PFA for 2 hr at 4 °C, washed with PBS, submerged in 30% sucrose overnight and embedded in OCT. Cryosections of 7 μm were dried for 1 hr at room temperature and rehydrated in PBS containing 0.1% fatty acid-free BSA for 10 min. To track the position of GFP-transduced B cells, a solution consisting of 1% NMS and 1:100 AF488-conjugated rabbit anti-GFP (Invitrogen, Cat#A21311), 1:100 biotin-conjugated anti-mouse CD35/CR1 (BD Bioscience, Cat # 553816), and 1:100 AF647-conjugated anti-mouse IgD (Biolegend, Cat#405708) was used to label transduced B cells, FDCs, and endogenous naive B cells, respectively. To examine the GC

confinement of endogenous mouse B cells, a solution consisting of 1% NMS and 1:100 biotin-conjugated GL7 (Thermofisher, Cat#13-5902-81) and 1:100 AF647-conjugated anti-mouse IgD (Biolegend, Cat#405708) was used to label GC B cells and naïve B cells, respectively. These solutions were incubated with the slides overnight at 4°C. The slides were then washed in PBS and stained with AF555-conjugated streptavidin (Life Technologies, Cat#S-21381) for 1 hr at room temperature, and images were captured with a Zeiss AxioObserver Z1 inverted microscope. For the assessment of P2RY8 effects on cell distribution within spleen and LNs, we compared sections that contained similar frequencies of transferred empty vector or P2RY8 transduced cells.

Two photon microscopy

EV- and P2RY8-transduced polyclonal B cells were counted and injected at equal numbers into separate wildtype mice, up to 60 mil GFP+ cells per mouse. Alternatively, the EV+ cell culture was labeled with CTV at 1:4000 and mixed such that there was a 1:1 ratio of EV+ to P2RY8+ cells. Up to 60 mil total EV-GFP+ and P2RY8-GFP+ cells of this mixture were injected into a single mouse. 24 hours later, tetramethylrhodamine conjugated dextran (MW 144 KDa or MW 2000 KDa, Sigma) was injected via retroorbital iv injection, five minutes after which the mouse was euthanized. After the skull was shaved and remaining hair was removed with a depilatory, an approximately 1.5cm incision was made in the skin and an O-ring was mounted to the skull using Vetbond tissue glue. This chamber was filled with water and then deep-tissue image acquisition of the calvaria was performed with ZEN2009 (Carl Zeiss, Germany) using a 7 MP two-photon microscope (Carl Zeiss) equipped with a Chameleon laser (Coherent).

A wavelength of 910nm was used to visualize GFP, tetramethylrhodamine and second harmonics, and a wavelength of 800nM to visualize CTV. Emission filters were 500–550 nm for GFP, 570–640 nm for tetramethylrhodamine, and 450–490 for CTV. Imaging was limited to approximately 1hr to ensure the dextran vasculature signal was maintained. For mixed transfer experiments, regions were selected to image by scanning through the tissue at 910nm, the wavelength at which the GFP but not CTV signal could be assessed. This ensured a non-biased approach to image acquisition.

Single plane images at wavelengths of 910nm and 800nm were combined and aligned using Imaris software (v.9.6). A grid was applied to each image to ensure accurate assessment of all cells in the image, and each visible cell was classified as either outside the vasculature, or inside/directly adjacent to the vasculature. Any pixel overlap with the dextran signal was classified as inside/directly adjacent to the vasculature. Following transduction EV+ and P2RY8+ B cell cultures expressed a range of GFP+, and analysis of cell localization 24hrs after transfer led to a degree of in vivo B cell proliferation, necessitating careful inspection in Imaris of each cell to check for any level of GFP+ and any level of CTV labeling. True fluorescence was distinguishable from macrophage autofluorescence due to the autofluorescence appearing in all channels acquired, and the elongated or punctal shape of the autofluorescence. Any regions that were imaged twice were excluded to ensure each cell was only counted once in the quantification. For quantification of images from mice that received only EV+ or only P2RY8+ cells, the quantification was done blinded, with file names coded before analysis. A total of 2528 cells were assessed across 10 experimental mice for the single

transfer analysis, and a total of 1761 cells were assessed across 4 experimental mice for the mixed transfer analysis. Total cells inside and directly adjacent to the vasculature were summed for each cell type in the transfer and divided by total cells of that type. This ratio was plotted for each experimental transfer, as can be seen in Supplementary Figure 2.7b.

Cell lines and treatments

HEK293T were grown in 10-cm tissue culture dishes in DMEM containing 10% FBS, 10 mM HEPES, 2 mM glutamine and 50 IU penicillin/streptomycin. WEHI-231 cells expressing P2RY8-GFP were grown in upright T25 flasks in RPMI containing 10% FBS, 10 mM HEPES, 2 mM glutamine, 55 μM 2-mercaptoethanol and 50 IU penicillin/streptomycin. All cell lines were previously obtained from other laboratories and further authentication was not performed. The cell lines were not tested for mycoplasma contamination.

To test bioactivity production, HEK293T cells were plated out in either 12-well or 6-well plates and allowed to reach confluence. The medium was then replaced with serum-free medium (RPMI containing 0.5% fatty acid-free BSA, 10 mM HEPES and 50 IU penicillin/streptomycin) at 750 μl per well for a 12-well plate or 1.5 ml per well for a 6-well plate. To this media was added either Abcc1 inhibitor MK571 (Caymen Chemical, Cat #70720) to a concentration of 50μM, or an equivalent volume of DMSO. The cells were incubated for 16 hr and then the supernatant was collected and centrifuged to

remove cells and debris. The supernatant was diluted 1:10 in migration assay media, mixed with CXCL12 and tested in the bioassay.

Migration inhibition transwell bioassay

A confluent T25 flask containing a mixture of wild-type and P2RY8-GFP-transduced WEHI-231 cells was washed twice in pre-warmed migration medium (RPMI containing 0.5% fatty acid-free BSA, 10 mM HEPES and 50 IU penicillin/streptomycin). The cells were resuspended in migration medium at 2×10^6 cells/ml and incubated for 10 min in a 37°C water bath. Recombinant human CXCL12 (Peprotech) was diluted to 50 ng/ml in migration medium. HEK293T cell supernatants were diluted at 1:10 concentration in the CXCL12-containing migration medium, and 600 µl of each of these mixtures was added to a 24-well tissue culture plate. Transwell filters (6 mm insert, 5 µm pore size, Corning) were placed on top of each well, and 100 µl of P2RY8-GFP-expressing WEHI-231 cells (2×10^5 cells) was added to the transwell insert. The cells were allowed to migrate for 3 h, after which the cells in the bottom well were counted by flow cytometry. To assess migration inhibition, the proportion of P2RY8-GFP+ cells that migrated for each well was divided by the proportion of P2RY8-GFP+ cells that migrated to CXCL12 alone. This normalized metric is plotted as 'P2RY8+ cells that migrate to CXCL12 (%).'

Migration assay of human T Cells

CRISPR edited human T cells were collected 3 days after editing. P2RY8 KO cells were labeled with 1:2000 CFSE (Invitrogen) and AAVS KO control cells were labeled with 1:2000 CTV (Fisher) and then mixed at a 1:1 ratio. In some experiments this labeling

was reversed. The cells were resuspended in migration medium at approximately 2 × 106 cells/ml and resensitized for 10 min in a 37°C water bath. Recombinant human CXCL12 (Peprotech) was diluted to 100 ng/ml in migration medium and synthetic GGG was added to aliquots via serial dilution from 1μM down to 10nM GGG. Transwell assays were performed as described in Supplementary Methods. To assess migration inhibition, the number of P2RY8 KO and AAVS KO cells that migrated to the bottom of each well was compared to the number of P2RY8 KO and AAVS KO cells that migrated to CXCL12 alone. The number of P2RY8 KO cells was also directly compared in a ratio to the number of AAVS KO cells that migrated in each well, a value that was normalized to the ratio in the wells receiving CXCL12 alone.

Immunizations, intravascular labeling and tissue collection

All immunizations were performed with intraperitoneal injection of 2x108 SRBC (Colorado Serum Company) in a volume of 400 μL. For studies of polyclonal P2RY8+ cell localization in the spleen or homing to the BM, mice were immunized on Day 0, cells were transferred in on Day 5, and tissues were harvested on Day 6 (or Day 11 for the analysis of T cells 5 days after transfer). For studies with chimeric mice in which Abcc1+/+ or -/- BM had been transduced with EV-GFP or P2RY8-GFP and used to reconstitute congenically marked recipients, mice were immunized with SRBC on Day 0 and Day 7, and then tissues were harvested on Day 10. In vivo pulse labeling was with 1 μg of PE-conjugated anti-CD45.2 injected i.v., and mice were analyzed after 3 min. Immune cells from spleen, mLNs, BM, PPs and blood were isolated as previously

described (Green et al., 2011). Lymph was collected from the cisterna chyli via fine glass micropipette as previously described(Matloubian et al., 2004).

CRISPR T Cell knockdown and adoptive transfer

Primary human CD3+ T cells were isolated by negative selection (Stemcell Technologies) from leukoreduction packs from healthy blood donors (Stemcell Technologies or Allcells Inc) under a protocol approved by the University of California San Francisco Institutional Review Board (IRB). Bulk CD3+ T cells were activated in X-Vivo-15 medium (Lonza) with 5% FBS, 50uM 2-ME, 10mM NAC, anti CD3/CD28 Dynabeads (Thermo), and a cytokine cocktail of IL-2 (300U/mL), IL-7 (5 ng/mL), and IL-15 5ng/mL). After 2 days of activation and culture, beads were removed by magnetic separation. In a 96-well format 4D-Nucleofector (Lonza), 1x106 cells were mixed with 50pmol of polymer-enhanced Cas9 ribonucleoproteins as previously described (Nguyen et al., 2020) with Edit-R synthetic guide RNA (Horizon Discovery), and electroporated with code EH-115. Cells were further cultured for 4 days post-editing in growth media with IL-2 (500U/mL), then an aliquot of cells was set aside for genomic DNA extraction, PCR, and Sanger sequencing to determine editing efficiency quantified by TIDE analysis (tide.nki.nl) as previously described (Brinkman et al., 2014). Target crRNA sequences and PCR primers are listed in Supplementary Table 2.1. CRISPR edited P2RY8 KO and AAVS KO control human T cells were labeled with CFSE and CTV and mixed at a 1:1 ratio. Cells were resuspended at 20mil cells/400µl saline and injected iv into NSG mice.

Cell surface flow cytometry staining

Cells were washed with FACS buffer (PBS containing 2% FBS and 1mM EDTA). Fc receptors were blocked by pre-incubating cells with 1:100 anti-CD16/CD32 (BioXCell, Cat#BE0307) for mouse cells or 1:100 TrueStain FcX (Biolegend, Cat#422303) for human cells, and cell viability determination was performed using LIVE/DEAD fixable stains (eBioscience Cat# 65-0865-18 or eBioscience Cat# 65-0864-14). Cells were stained with antibody cocktails for 30 minutes at 4℃, after which cells were washed twice with FACS buffer and analyzed by BD LSRII or Fortessa cell analyzer.

P2RY8 protein flow cytometry staining

Cells were fixed with 1.6% PFA (ThermoFisher) for 10 minutes at room temperature after LIVE/DEAD staining. Fixed cells were washed and permeabilized with Intracellular stain perm buffer (Invitrogen). Cells were intracellularly stained with 1:100 rabbit anti-human-P2RY8 in perm buffer for 1 hr at room temperature, washed twice with perm buffer, incubated for 30 min at room temperature with surface markers and 1:200 goat anti-rabbit IgG in perm buffer, washed again two times with perm buffer, and then resuspended in FACS buffer for analysis on a BD LSRII.

Flow cytometry antibodies

See Supplementary Table 2.2 for antibodies used. Flow cytometry data were analyzed using Flowjo (v.10.7.1).

Statistics

Prism software (GraphPad v.8.4.2) was used for all statistical analyses. The statistical tests used are specified in the figure legends. Two-tailed unpaired t-tests were performed when comparing only two groups, and ordinary one-way ANOVA using Tukey's multiple comparisons test was performed when comparing one variable across multiple groups. A two-tailed paired t-test was performed when comparing paired BM and blood samples from NSG mice that received CRISPR-edited human T cells. In summary graphs, points indicate individual samples and horizontal lines are means. Levels of significance were defined as *P < 0.05, **P < 0.01, ***P < 0.001, ****P < 0.0001.

GGG extraction and mass spectrometry

GGG was measured in the supernatant of cell cultures and tissue using the previously described LC-MS/MS protocol (Lu et al., 2019). For bile GGG measurements, to standardize the volume of bile among mice, food was removed from the cage for eight hours, and raw mouse bile was collected from the gallbladder using a syringe and flash frozen in liquid nitrogen until the time of measurement. Upon thawing, the bile was diluted 1:100 in MeOH and centrifuged at 4˚C for 30 min at 16,000 g to remove precipitate. The resulting MeOH supernatant was then analyzed LC-MS/MS. Mouse spleens and mouse BM flushed from a single femur and tibia were collected and individually weighed to allow for homogenization in 1:10 w/v 100% MeOH using a Precellys 24-bead homogenizer pre-cooled with dry ice. 15 µl of a 150 nM solution of leukotriene C4-d5 (LTC4-d5) (Caymen Chemical) was added to the homogenization as

an internal standard. The homogenate was transferred to a new tube. Then, 500 µl MeOH was used to wash the beads and was combined with the homogenate. The mixture was centrifuged for 30 min at 16,000 g in a microcentrifuge and the supernatant was diluted tenfold in water containing 3 mM HCl. Supernatant from five spleens of each genotype were pooled together then bound to a 500-mg C18 SPE column (Agilent Technologies), washed with 50% MeOH, eluted with MeOH, dried, and reconstituted in 200 µl of MeOH for LC-MS/MS analysis. Supernatant from each mouse BM sample was bound to a 500-mg C18 SPE column (Thermofisher), washed with 50% MeOH, eluted with MeOH, dried, and reconstituted in 200 µl of MeOH for LC-MS/MS analysis.

Human whole BM fresh aspirate was purchased from AllCells Inc in 3 ml aliquots from both male and female healthy donors between the ages of 27-38. Aspirate was collected in the afternoon with 78 IU/mL (nominal) porcine heparin anti-coagulant (Sagent Cat# 400-10) and shipped overnight for processing the next morning. Aspirate was diluted with 10ml of PBS and centrifuged at 4˚C for 5 min at 1500 rpm twice to pellet cells, with the supernatant moved into a fresh tube each time. Following these two spins, the supernatant was centrifuged for a third time at 4˚C for 10min at 9500 rpm, after which it was acidified to pH 3 with 3M HCl and 15 µl of a 150 nM solution of LTC4-d5 was added. This solution was then processed on a C18 SPE column identically to that of the spleen extract described above.

Polyclonal B cell cultures were activated under conditions analogous to those detailed for B cell retroviral transduction, and after 72 hrs the supernatants were collected and

centrifuged to remove cells and debris. 3M HCl was added to a pH of 3, and the supernatants were frozen in liquid nitrogen until time of processing. Upon thawing, MeOH was added to form a 20% MeOH solution, and 10 nM of the internal standard LTC4-d5 was added. The resulting solution was bound to a C18 SPE column and processed identically to the spleen and human BM extracts described above, except the column was not washed with a 50% MeOH solution, rather GGG was directly eluted in 100% MeOH.

A Shimadzu Nexera X2 HPLC coupled to an AB SCIEX QTRAP 6500 mass spectrometer was used for LC-MS analysis of B cell culture supernatant, mouse spleens, and human BM. Use of a more sensitive AB SCIEX QTRAP 7500 instrument allowed for measurement of mouse BM bound to a C18 SPE column, for which tissue volume was limited. 10µl of each sample was injected onto a Synergi Polar-RP column (75 × 4.6 mm) and a mobile phase gradient consisting of A: H2O + 0.1% formic acid; and B: acetonitrile + 0.1% formic acid. 0–1 min, 40% B; 1–4 min, ramp to 95% B; 4–6 min, 95% B; 6–6.5 min, ramp to 50% B; 6.5–8 min, 40% B was used for analysis. GGG was detected in positive ionization mode using multiple reaction monitoring scans with ion pair m/z 580.3/179.0. The internal standard, LTC4-d5, was identified with ion pair m/z 631.4/179.0. The turbo spray ion source was maintained at 44°C, 20 CUR, 40 GS1 and 40 GS2, 5,500 IS, with compound settings DP 160, EP 10, and CXP 10. A collision energy of 35 eV was used when performing fragmentation analysis. Peak area was integrated using Sciex Analyst software and referenced against a standard curve prepared with 0.1, 1, 10, 100, 1000 nM synthetic GGG to calculate compound

abundance. Feature area intensities were scaled to the mass of sample where relevant, with 1g of sample equated to 1mL for the calculation of molarity.

Acknowledgments:

For access to μMT mice and Nod scid gamma mice we thank C. Allen and Q. Tang at UCSF, respectively. For advice regarding calvaria imaging, we thank Joao Pereira.

Funding:

This work was funded by National Institute of Allergy and Infectious Disease grant to A.E.G. (F30AI150061). F.D.W. is supported by a CRI Irvington postdoctoral fellowship. D.N.N. is supported by NIH grants L40AI140341 and K08AI153767 and the CIRM Alpha Stem Cell Clinic Fellowship. A.M. holds a Career Award for Medical Scientists from the Burroughs Wellcome Fund, is an investigator at the Chan–Zuckerberg Biohub and is a recipient of The Cancer Research Institute (CRI) Lloyd J. Old STAR grant. The Marson lab has received funds from the Innovative Genomics Institute (IGI) and the Parker Institute for Cancer Immunotherapy (PICI). J.G.C. is an HHMI investigator, recipient of a UCSF PBBR Award, and is also supported by a National Institutes of Health USA Grant (R01 AI045073).

Competing interests:

The authors declare no competing interests. Data and materials availability: All data needed to evaluate the conclusions in the paper are present in the paper or the Supplementary Materials.

CHAPTER THREE

Conclusion

Discussion

In this study we define key requirements for the establishment of extracellular GGG distribution in lymphoid tissues. We show that GGG is an endogenous substrate for cell membrane transporter Abcc1 and that Abcc1 is used by both hematopoietic and non-hematopoietic cells to export GGG. Additionally, we show that Ggt5 is necessary for extracellular GGG catabolism in lymphoid tissues. Our data indicate that Abcc1 and Ggt5 act in concert to support P2RY8-mediated confinement of cells to the GC, and Abcc1 is also needed for growth regulation of P2RY8+ GC B cells. Furthermore, we show that extracellular GGG is generated in an Abcc1-dependent manner in the BM, and we provide evidence that P2RY8 can restrict lymphocyte accumulation in the BM parenchyma (**Figure 3.1**).

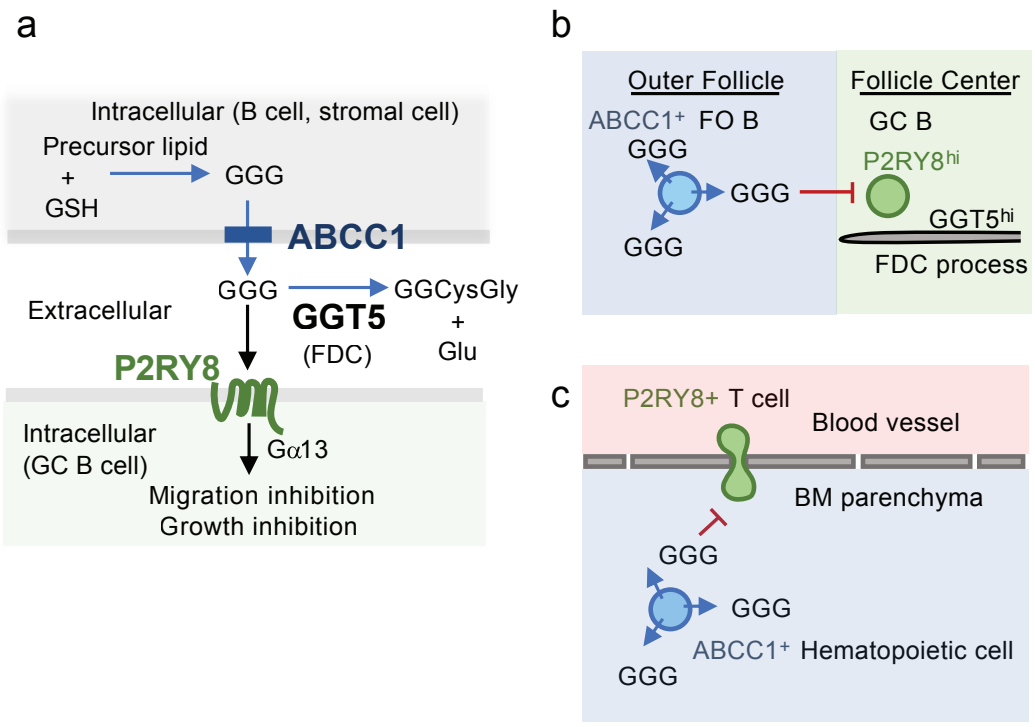

Figure 3.1: Model diagrams summarizing ABCC1 and GGT5 function in determining GGG distribution and P2RY8+ cell behavior.
Diagrams showing: (a) Role of ABCC1 in GGG export from cells, action on P2RY8+ target cells and catabolism in the extracellular space by GGT5; (b) follicular B cells exporting GGG in an ABCC1-dependent manner and confining P2RY8hi GC B cells to the GGT5hi FDC network at the follicle center; (c) an adherent P2RY8+ T cell in a BM blood vessel being inhibited in transmigration (or promoted to undergo reverse transmigration) by GGG produced by ABCC1+ hematopoietic cells in the BM parenchyma.

Earlier work (Lu et al., 2019) established that although rodents lack P2RY8, they produce the P2RY8 ligand GGG, a finding that we build on here. We make the inference that the GGG-P2RY8 pathway functions in humans in a manner that is closely modeled by our studies in the mouse for the following reasons. First, P2RY8 loss-of-function mutations in lymphoma patients are associated with GC B cell over-growth and dissemination, leading to the prediction that P2RY8 promotes GC B cell growth restraint

and confinement; we observe that P2RY8 is sufficient to have these effects in the mouse. Second, Ggt5 expression by FDCs is conserved between humans and mice (Lu et al., 2019). Third, Abcc1 is widely expressed by human immune cells, similar to its expression in the mouse. Finally, our mass spectrometry measurements have shown comparable GGG abundance in mouse lymph nodes and human tonsil (Lu et al., 2019) and that GGG is present in mouse and human BM. Taken together, these observations suggest efforts to decipher the biology of this ligand-receptor system using mouse models will help illuminate the role of P2RY8 in human physiology and disease.

Despite the lack of a clear P2RY8 orthologue in mice, the GGG gradient has been maintained evolutionarily, with the conserved expression of Ggt5 and Abcc1 in similar cell types as seen in humans. Studies from our lab have suggested that in addition to S1PR2, there is a second Gα13-coupled receptor that acts via an FDC-dependent circuit to support the confinement of endogenous mouse B cells (Wang et al., 2011) (Muppidi et al., 2015). However, our results here demonstrate that murine GC B cells do not require the GGG gradient for their confinement in the spleen or lymph nodes, suggesting that the receptor mediating this further confinement of murine B cells is not a P2RY8-related receptor responding to GGG. Future studies will work to identify this receptor, as like S1PR2 and P2RY8, it may contribute to human disease.

Despite the lack of a clear murine P2RY8 orthologue, the GGG gradient has been maintained evolutionarily in mice, with the expression of Ggt5 and Abcc1 mirroring the pattern of expression seen in humans. Studies from our lab have suggested that in

addition to S1PR2, there is a second Gα13-coupled receptor that acts via an FDC-dependent circuit to support the confinement of endogenous mouse B cells (Wang et al., 2011) (Muppidi et al., 2015). However, our results here demonstrate that this receptor is unlikely to be a P2RY8-related receptor responding to GGG, as murine GC B cells do not require the GGG gradient for their confinement in the spleen or lymph nodes. Future studies will work to identify this confinement receptor, as its dysregulation may contribute to human disease, as is the case for S1PR2 and P2RY8.

ABCC1 is intensely studied for its ability to transport a diversity of drugs and xenobiotics, often as glutathione conjugates, though it has only one well-defined endogenous substrate in vivo, LTC4 (Cole, 2014). We now add GGG as another endogenous substrate of ABCC1. ABCC1 transporter activity is not known to be regulated or gated beyond its ATP requirement (Cole, 2014) (Wiese and Stefan, 2019). Instead, the expression pattern of the transporter is likely to be a key determinant of where GGG export occurs. The widespread expression of ABCC1 suggests that most cell types within lymphoid tissues have the capacity to export GGG. The key factors determining GGG distribution may then be the enzymes involved in GGG synthesis and degradation. While our gene knockout data show a critical role for Abcc1 in generating extracellular GGG in lymphoid tissues that can act on P2RY8, we continue to observe significant amounts of GGG in the bile of Abcc1-deficient mice, likely indicating that at least one additional Abcc transporter is active in GGG export. In this regard, it is notable that Abcc2 and Abcc3, close homologs of Abcc1, are particularly abundant in the liver (BioGPS.org).

We show that follicular B cells are a necessary source of GGG to mediate the GC confinement of P2RY8+ B cells, identifying a form of crosstalk between different B cell subsets in lymphoid tissues. In mice lacking Abcc1 only in hematopoietic cells or fully deficient in B cells, P2RY8+ B cells were not confined to GCs but they were also not uniformly distributed in follicles; rather they had a propensity to distribute at the follicle-GC boundary. We speculate that under normal conditions, follicular GGG is produced by B cells and stromal cells, and this achieves a high concentration that penetrates some distance into the Ggt5+ FDC network that occupies the GC. This 'gradient' helps promote confinement of P2RY8+ cells within the GC. When stromal cells are the only source of GGG, the lower amounts of GGG may be more readily degraded by the Ggt5+ FDCs with little penetration into the GC. Under these conditions P2RY8 is only sufficient to position activated B cells at the follicle-GC interface.

Within lymphoid follicles, Ggt5 is most highly expressed by FDCs. The previous finding that FDCs are required for P2RY8-mediated confinement of cells to the follicle center and to GCs (Muppidi et al., 2015) is consistent with them having a critical role in GGG catabolism. Ggt5 is also detectable on stromal cells in the T zone of LNs and human tonsil (Lu et al., 2019), and the transcript is present in naïve T cells and dendritic cells (Immgen.org). Whether GGG-P2RY8 signaling has a role in regions of secondary lymphoid tissue outside the follicle has not yet been determined. We speculate that GGG distribution may also be tightly regulated in the T zone, allowing GGG to influence cell compartmentalization within this zone. Moreover, while we establish that Ggt5 has a

non-redundant role in catabolism of GGG in lymphoid tissues, our findings do not exclude possible contributions by other Ggt family members in GGG catabolism.

Abcc1 and Ggt5 regulation of cell trafficking to the BM identifies a role for P2RY8 outside the GC. The BM is a significant site of lymphocyte and plasma cell homing. Multiple studies have characterized the presence of memory T cells in mouse and human BM, and it has been suggested that they are an important memory reservoir in both protective and autoimmune contexts (Di Rosa and Gebhardt, 2016) (Collins et al., 2019) (Mazo et al., 2005). The intravascular labeling experiments presented here indicate that P2RY8-expressing cells are ultimately impeded in their movement from blood vessels into the BM parenchyma, failing to accumulate in the parenchyma after 24hrs. VCAM1 is required for homing of circulating B and T cells into the BM, facilitating the adherence of lymphocytes to the vessel wall (Koni et al., 2001) (Mazo et al., 2005). The requirements for lymphocyte transendothelial migration into the BM after sticking are not fully characterized, but CXCR4 and CXCL12 play a role in this process (Mazo et al., 2005). In accord with P2RY8's established role in inhibiting migration towards chemoattractants, we speculate that P2RY8 may act to antagonize the transmigration step, counteracting the influence of chemoattractants and thereby gating lymphocyte access to the BM. It may also be the case that P2RY8-expressing cells encounter GGG after they have migrated through the endothelium, leading them to reverse transmigrate back into the vasculature. In addition to their role in lymphocyte transmigration, CXCR4 and CXCL12 are also important in homing of plasma cells to the BM (Cyster, 2003). It will be important in future work to determine if newly generated human plasmablasts

express sufficient amounts of P2RY8 to potentially restrict their accumulation in the BM and to understand what factors alter P2RY8 expression in BM tropic cells. Additionally, while we focused our homing studies on the BM, our finding that P2RY8 expression reduced homing to the spleen suggests the receptor may restrain P2RY8+ cell accumulation in other tissues.

The widespread expression of P2RY8 in human BM cells detected by scRNAseq analysis (Hay et al., 2018) suggests that this receptor may have broad influences on cell distribution in this compartment. This includes not only high expression in CD8 T cells, NK cells and mature B cells, but also in early hematopoietic progenitors and pre-B cells. The expression by pre-B cells is notable, as fusions of the P2RY8 gene with the CRLF2 gene (encoding a component of the TSLP receptor) are recurrent in B-progenitor acute lymphoblastic leukemia (ALL) (Mullighan et al., 2009). High P2RY8 expression at this developmental stage may contribute to over-expression of the TSLP receptor from the fusion locus. It is notable that Ggt5 is largely restricted to stromal cells within the BM. A scRNAseq study of human BM stromal cells identified 9 subsets, and Ggt5 was present in subsets 1 and 7 (Baryawno et al., 2019). These two subsets were also the most enriched for CXCL12. Therefore, P2RY8 may help mediate confinement of CXCR4+ cells in association with these stromal cells due to Ggt5 establishing a GGG-low niche in their proximity. Additionally, expression of P2RY8 on maturing B cells may contribute to their movement away from certain BM niches where GGG may be high and thereby favor their movement into blood. Beyond effects on confinement, GGG-P2RY8 signaling in BM progenitors and lymphocytes is expected to restrain signaling via the AKT

pathway and to transmit other Rho-dependent signals. Since PI3K and AKT signaling has important roles in B cell development and selection (Clark et al., 2014) (Lau et al., 2020), the GGG-P2RY8 axis may exert significant influence over these events.

P2RY8 and GNA13 are frequently mutated in GC-derived lymphomas (Muppidi et al., 2014) (Lohr et al., 2012) (Morin et al., 2013) (Forbes et al., 2011) (Schmitz et al., 2018) (Kridel et al., 2016). The Abcc1 dependence of the growth repressive influence of P2RY8 on GC B cell responses is consistent with GGG acting in vivo on GC B cells to repress Akt (and possibly other pro-growth signaling pathways). It is notable that GC-derived lymphomas retain an extensive FDC network at least through the early stages of disease (Carbone and Gloghini, 2014). A large FDC network would be expected to maintain low GGG levels, acting as an alternative mechanism to P2RY8 or GNA13 mutation to limit P2RY8-mediated repression of growth-promoting pathways. BM involvement presents in a portion of GCB-DLBCL patients and is a predictor of poor clinical outcome (Sehn et al., 2011). Mutations in P2RY8 and GNA13 may not only lead to loss of GC confinement and GC B cell growth regulation, but also favor the recruitment of malignant cells to the BM. In another cancer context, efforts are being pursued to antagonize the multidrug transporter activity of ABCC1 in an attempt to improve the success of chemotherapies (Cole, 2014) (Kunická and Souček, 2014). The role of ABCC1 in transporting GGG will be important to consider in the context of these efforts. It will also be of interest to determine whether the polymorphisms that have been described in ABCC1 (Kunická and Souček, 2014) (Yin and Zhang, 2011) lead to alterations in GGG export. The basis for the stronger effect of P2RY8 in restraining GC

B cell growth in PPs than in spleen and mLNs is not yet known but is in accord with earlier findings (Muppidi et al., 2014). We speculate that different combinations of factors may contribute to GC growth control in different lymphoid organs. Moreover, it should be kept in mind that the mouse model may only be effective in revealing a fraction of P2RY8's endogenous functions in humans. For example, the importance of P2RY8 in human LNs is strongly suggested by the evidence that GCB-DLBCL and BL frequently emerge in these tissues (Carbone et al., 2009).

Finally, while we highlight influences of the P2RY8-GGG axis on lymphocyte organization in secondary lymphoid organs and trafficking to the BM, we note that ABCC1 is widely expressed in tissues and GGG can be made by many cell and tissue types (Lu et al., 2019). Therefore, the findings described here are anticipated to provide a foundation for understanding the broader influences of GGG and P2RY8 in the human immune system.

REFERENCES

Baryawno, N., Przybylski, D., Kowalczyk, M.S., Kfoury, Y., Severe, N., Gustafsson, K., Kokkaliaris, K.D., Mercier, F., Tabaka, M., Hofree, M., et al. (2019). A Cellular Taxonomy of the Bone Marrow Stroma in Homeostasis and Leukemia. Cell *177*, 1915–1932.e1916.

Brinkman, E.K., Chen, T., Amendola, M., and van Steensel, B. (2014). Easy quantitative assessment of genome editing by sequence trace decomposition. Nucleic Acids Res *42*, e168.

Carbone, A., and Gloghini, A. (2014). Follicular dendritic cell pattern in early lymphomas involving follicles. Adv Anat Pathol *21*, 260–269.

Carbone, A., Gloghini, A., Cabras, A., and Elia, G. (2009). The Germinal centre-derived lymphomas seen through their cellular microenvironment. Br J Haematol *145*, 468–480.

Carter, B.Z., Wiseman, A.L., Orkiszewski, R., Ballard, K.D., Ou, C.N., and Lieberman, M.W. (1997). Metabolism of leukotriene C4 in gamma-glutamyl transpeptidase-deficient mice. J Biol Chem *272*, 12305–12310.

Chen, S., Lee, B., Lee, A.Y.-F., Modzelewski, A.J., and He, L. (2016). Highly Efficient Mouse Genome Editing by CRISPR Ribonucleoprotein Electroporation of Zygotes. J Biol Chem *291*, 14457–14467.

Chen, X.S., Sheller, J.R., Johnson, E.N., and Funk, C.D. (1994). Role of leukotrienes revealed by targeted disruption of the 5-lipoxygenase gene. Nature *372*, 179–182.

Chun, J., Hla, T., Lynch, K.R., Spiegel, S., and Moolenaar, W.H. (2010). International Union of Basic and Clinical Pharmacology. LXXVIII. Lysophospholipid receptor nomenclature. Pharmacol Rev *62*, 579–587.

Clark, M.R., Mandal, M., Ochiai, K., and Singh, H. (2014). Orchestrating B cell lymphopoiesis through interplay of IL-7 receptor and pre-B cell receptor signalling. Nature Reviews Immunology *14*, 69–80.

Cole, S.P.C. (2014). Targeting multidrug resistance protein 1 (MRP1, ABCC1): past, present, and future. Annu Rev Pharmacol Toxicol *54*, 95–117.

Collins, N., Han, S.-J., Enamorado, M., Link, V.M., Huang, B., Moseman, E.A., Kishton, R.J., Shannon, J.P., Dixit, D., Schwab, S.R., et al. (2019). The Bone Marrow Protects and Optimizes Immunological Memory during Dietary Restriction. Cell *178*, 1088–1101.e15.

Cyster, J.G. (2003). Homing of antibody secreting cells. Immunological Reviews *194*, 48–60.

Cyster, J.G., and Allen, C.D.C. (2019). B Cell Responses: Cell Interaction Dynamics and Decisions. Cell *177*, 524–540.

Di Rosa, F., and Gebhardt, T. (2016). Bone Marrow T Cells and the Integrated Functions of Recirculating and Tissue-Resident Memory T Cells. Front. Immunol. *7*, 51.

Forbes, S.A., Bindal, N., Bamford, S., Cole, C., Kok, C.Y., Beare, D., Jia, M., Shepherd, R., Leung, K., Menzies, A., et al. (2011). COSMIC: mining complete cancer genomes in the Catalogue of Somatic Mutations in Cancer. Nucleic Acids Res *39*, D945–D950.

Green, J.A., Suzuki, K., Cho, B., Willison, L.D., Palmer, D., Allen, C.D.C., Schmidt, T.H., Xu, Y., Proia, R.L., Coughlin, S.R., et al. (2011). The sphingosine 1-phosphate receptor $S1P_2$ maintains the homeostasis of germinal center B cells and promotes niche confinement. Nature Immunology *12*, 672–680.

Hay, S.B., Ferchen, K., Chetal, K., Grimes, H.L., and Salomonis, N. (2018). The Human Cell Atlas bone marrow single-cell interactive web portal. Exp Hematol *68*, 51–61.

Hayes, J.D., Flanagan, J.U., and Jowsey, I.R. (2004). GLUTATHIONE TRANSFERASES. Annu Rev Pharmacol Toxicol *45*, 51–88.

Heisterkamp, N., Groffen, J., Warburton, D., and Sneddon, T.P. (2008). The human gamma-glutamyltransferase gene family. Hum Genet *123*, 321–332.

Koley, D., and Bard, A.J. (2012). Inhibition of the MRP1-mediated transport of the menadione-glutathione conjugate (thiodione) in HeLa cells as studied by SECM. Proc Natl Acad Sci USA *109*, 11522.

Koni, P.A., Joshi, S.K., Temann, U.A., Olson, D., Burkly, L., and Flavell, R.A. (2001). Conditional vascular cell adhesion molecule 1 deletion in mice: impaired lymphocyte migration to bone marrow. J Exp Med *193*, 741–754.

Kridel, R., Chan, F.C., Mottok, A., Boyle, M., Farinha, P., Tan, K., Meissner, B., Bashashati, A., McPherson, A., Roth, A., et al. (2016). Histological Transformation and Progression in Follicular Lymphoma: A Clonal Evolution Study. PLoS Med *13*, e1002197.

Kunická, T., and Souček, P. (2014). Importance of ABCC1 for cancer therapy and prognosis. Drug Metab Rev *46*, 325–342.

Lau, A., Avery, D.T., Jackson, K., Lenthall, H., Volpi, S., Brigden, H., Russell, A.J., Bier, J., Reed, J.H., Smart, J.M., et al. (2020). Activated PI3Kδ breaches multiple B cell tolerance checkpoints and causes autoantibody production. J Exp Med *217*.

Lee, J., Brehm, M.A., Greiner, D., Shultz, L.D., and Kornfeld, H. (2013). Engrafted human cells generate adaptive immune responses to Mycobacterium bovis BCG infection in humanized mice. BMC Immunol *14*, 53.

Leeman-Neill, R.J., and Bhagat, G. (2018). BCL6 as a therapeutic target for lymphoma. Expert Opin Ther Targets *22*, 143–152.

Li, Y., Masse-Ranson, G., Garcia, Z., Bruel, T., Kök, A., Strick-Marchand, H., Jouvion, G., Serafini, N., Lim, A.I., Dusseaux, M., et al. (2018). A human immune system mouse model with robust lymph node development. Nat Methods *15*, 623–630.

Lohr, J.G., Stojanov, P., Lawrence, M.S., Auclair, D., Chapuy, B., Sougnez, C., Cruz-Gordillo, P., Knoechel, B., Asmann, Y.W., Slager, S.L., et al. (2012). Discovery and prioritization of somatic mutations in diffuse large B-cell lymphoma (DLBCL) by whole-exome sequencing. Proc Natl Acad Sci U S A *109*, 3879–3884.

Lorico, A., Rappa, G., Finch, R.A., Yang, D., Flavell, R.A., and Sartorelli, A.C. (1997). Disruption of the murine MRP (multidrug resistance protein) gene leads to increased sensitivity to etoposide (VP-16) and increased levels of glutathione. Cancer Res *57*, 5238–5242.

Lu, E., and Cyster, J.G. (2019). G-protein coupled receptors and ligands that organize humoral immune responses. Immunological Reviews *289*, 158–172.

Lu, E., Wolfreys, F.D., Muppidi, J.R., Xu, Y., and Cyster, J.G. (2019). S-Geranylgeranyl-l-glutathione is a ligand for human B cell-confinement receptor P2RY8. Nature *567*, 244–248.

Matloubian, M., Lo, C.G., Cinamon, G., Lesneski, M.J., Xu, Y., Brinkmann, V., Allende, M.L., Proia, R.L., and Cyster, J.G. (2004). Lymphocyte egress from thymus and peripheral lymphoid organs is dependent on S1P receptor 1. Nature *427*, 355–360.

Mazo, I.B., Honczarenko, M., Leung, H., Cavanagh, L.L., Bonasio, R., Weninger, W., Engelke, K., Xia, L., McEver, R.P., Koni, P.A., et al. (2005). Bone marrow is a major reservoir and site of recruitment for central memory CD8+ T cells. Immunity *22*, 259–270.

Morin, R.D., Mungall, K., Pleasance, E., Mungall, A.J., Goya, R., Huff, R.D., Scott, D.W., Ding, J., Roth, A., Chiu, R., et al. (2013). Mutational and structural analysis of diffuse large B-cell lymphoma using whole-genome sequencing. Blood *122*, 1256–1265.

Mullighan, C.G., Collins-Underwood, J.R., Phillips, L.A.A., Loudin, M.G., Liu, W., Zhang, J., Ma, J., Coustan-Smith, E., Harvey, R.C., Willman, C.L., et al. (2009). Rearrangement of CRLF2 in B-progenitor- and Down syndrome-associated acute lymphoblastic leukemia. Nat Genet *41*, 1243–1246.

Muppidi, J.R., Lu, E., and Cyster, J.G. (2015). The G protein-coupled receptor P2RY8 and follicular dendritic cells promote germinal center confinement of B cells, whereas S1PR3 can contribute to their dissemination. J Exp Med *212*, 2213–2222.

Muppidi, J.R., Schmitz, R., Green, J.A., Xiao, W., Larsen, A.B., Braun, S.E., An, J., Xu, Y., Rosenwald, A., Ott, G., et al. (2014). Loss of signalling via Gα13 in germinal centre B-cell-derived lymphoma. Nature 1–18.

Nguyen, D.N., Roth, T.L., Li, P.J., Chen, P.A., Apathy, R., Mamedov, M.R., Vo, L.T., Tobin, V.R., Goodman, D., Shifrut, E., et al. (2020). Polymer-stabilized Cas9 nanoparticles and modified repair templates increase genome editing efficiency. Nature Biotechnology *38*, 44–49.

Schmitz, R., Wright, G.W., Huang, D.W., Johnson, C.A., Phelan, J.D., Wang, J.Q., Roulland, S., Kasbekar, M., Young, R.M., Shaffer, A.L., et al. (2018). Genetics and Pathogenesis of Diffuse Large B-Cell Lymphoma. N Engl J Med *378*, 1396–1407.

Schmitz, R., Young, R.M., Ceribelli, M., Jhavar, S., Xiao, W., Zhang, M., Wright, G., Shaffer, A.L., Hodson, D.J., Buras, E., et al. (2012). Burkitt lymphoma pathogenesis and therapeutic targets from structural and functional genomics. Nature *490*, 116–120.

Sehn, L.H., Scott, D.W., Chhanabhai, M., Berry, B., Ruskova, A., Berkahn, L., Connors, J.M., and Gascoyne, R.D. (2011). Impact of concordant and discordant bone marrow involvement on outcome in diffuse large B-cell lymphoma treated with R-CHOP. J Clin Oncol *29*, 1452–1457.

Shi, Z.Z., Han, B., Habib, G.M., Matzuk, M.M., and Lieberman, M.W. (2001). Disruption of gamma-glutamyl leukotrienase results in disruption of leukotriene D(4) synthesis in vivo and attenuation of the acute inflammatory response. Mol Cell Biol *21*, 5389–5395.

Shimizu, T. (2009). Lipid mediators in health and disease: enzymes and receptors as therapeutic targets for the regulation of immunity and inflammation. Annu Rev Pharmacol Toxicol *49*, 123–150.

Slot, A.J., Molinski, S.V., and Cole, S.P.C. (2011). Mammalian multidrug-resistance proteins (MRPs). Essays Biochem *50*, 179–207.

Sugimoto, Y., and Narumiya, S. (2007). Prostaglandin E receptors. J Biol Chem *282*, 11613–11617.

Victora, G.D., and Nussenzweig, M.C. (2012). Germinal Centers. Annu. Rev. Immunol. *30*, 429–457.

Wang, X., Cho, B., Suzuki, K., Xu, Y., Green, J.A., An, J., and Cyster, J.G. (2011). Follicular dendritic cells help establish follicle identity and promote B cell retention in germinal centers. J Exp Med *208*, 2497–2510.

Wiese, M., and Stefan, S.M. (2019). The A-B-C of small-molecule ABC transport protein modulators: From inhibition to activation-a case study of multidrug resistance-associated protein 1 (ABCC1). Med Res Rev *39*, 2031–2081.

Yin, J., and Zhang, J. (2011). Multidrug resistance-associated protein 1 (MRP1/ABCC1) polymorphism: from discovery to clinical application. Zhong Nan Da Xue Xue Bao Yi Xue Ban *36*, 927–938.

Publishing Agreement

It is the policy of the University to encourage open access and broad distribution of all theses, dissertations, and manuscripts. The Graduate Division will facilitate the distribution of UCSF theses, dissertations, and manuscripts to the UCSF Library for open access and distribution. UCSF will make such theses, dissertations, and manuscripts accessible to the public and will take reasonable steps to preserve these works in perpetuity.

I hereby grant the non-exclusive, perpetual right to The Regents of the University of California to reproduce, publicly display, distribute, preserve, and publish copies of my thesis, dissertation, or manuscript in any form or media, now existing or later derived, including access online for teaching, research, and public service purposes.

DocuSigned by:
Antonia Gallman
7A9ADD20262A465...
Author Signature

4/9/2021
Date